From electrons to stars : modelling and mitigation of radiation damage effects on astronomical CCDs

Prod'homme, T.

Chapter 6

Digging supplementary buried channels: Investigating the notch architecture within the CCD pixels on ESA's Gaia satellite

ESA's Gaia satellite has 106 CCD image sensors of a design that includes Supplementary Buried Channels (SBCs, otherwise known as 'notches') within the charge transfer channels or 'columns' to mitigate against the effects of radiation damage at low signal levels. The formally agreed CCD acceptance criterion in the Gaia contract between ESA/EADS Astrium and e2v only stipulated that SBCs should be present in Gaia CCDs but Kohley et al., in testing one Gaia Flight Model (FM), found that SBCs were present in only some of the pixels along every column. Missing SBCs will cause increased signal loss due to radiation damage and could thus degrade the predicted scientific performance of the mission. We re-analyse and model data from eight pre-2004 Gaia CCDs and find that one of these CCDs is missing some of its SBCs. Out of all the columns in these eight CCDs, less than 1% of columns are missing some SBCs. We obtain new measurements, re-analyse existing measurements and include a literature result for four post-2004 CCDs. Three of these have missing SBCs. Out of all the columns in these four CCDs, 68% of columns are missing some SBCs (all the FM CCDs are post-2004). The difference between these two samples is highly statistically significant and points to a change in e2v manufacturing of Gaia CCDs between 2003 and 2005. e2v predicts that all CCDs in the same batch should have the same SBC characteristics. By comparing the batch numbers of the three affected CCDs (three different batches) with those currently assigned to the Gaia satellite (it is too late to change them), we tentatively predict that a minimum of 17% of flight CCDs are likely to be affected by the SBC issue. In the absence of further testing, we predict that in the other 29 completely untested batches 69% of the CCDs may be affected (between 11 and 100% with a 99% confidence interval). Therefore it appears likely that the majority of Gaia's 106 CCDs have the same missing SBC issue as the two CCDs in Hubble's Advanced Camera for Surveys (ACS)/Wide Field Channel (WFC), albeit in only some of Gaia's pixels. We show that even with missing SBCs, Gaia astrometry still meets mission requirements. Simulations of whether Gaia photometry and spectroscopy still meet mission requirements in the absence of missing SBCs should be conducted. We recommend that SBC efficiency tests (described and used in this chapter) should be conducted: both pre-launch on-ground testing and post-launch in-flight testing.

G.M. Seabroke, T. Prod'homme, N.J. Murray, C. Crowley, G. Hopkinson, A.G.A. Brown, R. Kohley, A. Holland *To be submitted*

6.1 Introduction

ESA's Gaia satellite is a high-precision astrometric, photometric and spectroscopic ESA cornerstone mission, scheduled for launch in 2013, that will produce the most accurate stereoscopic map to date of the Milky Way. This will be achieved by measuring parallaxes, proper motions, radial velocities, and astrophysical parameters for one billion stars, one percent of the estimated stellar population in our Galaxy (Perryman et al. 2001). Figure 6 in Seabroke et al. (2008b) shows that Gaia observations will consist of charge packets within each CCD pixel ranging from one to the pixel full well capacity (FWC) of $190\,000$ electrons. This is due to Gaia's completeness range ($6 \leq V \leq 20$ mag) and the fixed exposure time for each CCD (4.4 s), due to operating in Time-Delayed Integration (TDI) mode in step with the satellite's spin rate. The vast majority of Gaia observations will be at the faint end of its magnitude range and correspondingly the vast majority of the charge packets that make up Gaia observations are expected to range from one to thousands of electrons. Gaia will operate in the radiation environment at L2 for at least five years. During the mission, radiation will generate 'traps' in the silicon which cause a loss of charge transfer efficiency (CTE) i.e. the fraction of the charge signal correctly transferred from pixel to pixel. The design of the Gaia CCDs includes Supplementary Buried Channels (SBCs) to confine charge signals to a small volume of silicon, thereby reducing the number of traps with which the signal can interact and maximising the CTE.

The formally agreed CCD acceptance criterion in the Gaia contract between ESA/EADS Astrium and e2v only stipulated that SBCs should be present in Gaia CCDs. This was demonstrated to be the majority case in CCDs built prior to 2004, Demonstrator Models (DMs, from the Technology Demonstration Activities (TDA) phase) and Engineering Models (EMs), by Hopkinson (2006) using the First Pixel Response (FPR) method, which can only be used on irradiated CCDs. Before manufacturing Flight Models (FMs), e2v changed their photo-lithographic mask set in 2004 but the set was meant to be identical to the one used to manufacture the DMs and EMs. FMs were not systematically tested for SBC efficiency. In an independent one-off test, Kohley et al. (2009) tested one close-reject FM and found SBCs are only present in some pixels along every CCD column. Note that this was not the reason for this particular FM not being selected for the actual mission. Also the method used here, pocket pumping, has the advantage of being able to be used on un-irradiated and irradiated CCDs.

Seabroke et al. (2010)'s 3D semi-conductor physics model of the Gaia pixel provided a manufacturing alignment explanation for why SBCs are only present in some pixels along a CCD column. An accumulation of nominal alignment errors, thought to be rare by e2v, can add up to the alignment error found in Seabroke et al. (2010) required to remove SBCs from some pixels along specific columns furthest from the readout register. However, Kohley et al. (2009) found SBCs are only present in some pixels along *every* CCD column. Given that the mask set changed in 2004, this chapter investigates whether there are systematic differences between the SBCs in pre- and post-2004 CCDs. The change in the mask set can only be considered as circumstantial evidence to explain any systematic changes between pre- and post-2004 CCDs because it would be very difficult to definitely prove the mask set was responsible due to a plethora of

other factors that go into manufacturing CCDs with complex pixel architectures.
The issue of missing or non-functional SBCs is not unique to Gaia. In spite of manufactured specifications and laboratory tests, SBCs in the two CCDs in Hubble's Advanced Camera for Surveys (ACS)/Wide Field Channel (WFC) are not behaving 'in-flight' as predicted. It was expected that below 100 electrons, Charge Transfer Inefficiency (CTI) in these detectors should have been mitigated. Instead CTI becomes worse with increasingly small charge packets (Anderson & Bedin 2010) suggesting that the SBCs are missing.
Similarly, missing SBCs would increase the effects of radiation damage on Gaia observations. This introduces a systematic bias in the measurements (e.g. image location on the CCD, radial velocities etc). As described in detail in Chapter 3 the Gaia data processing takes into account CTI effects via the forward modelling of the image distortion. This approach allows for the unbiased estimation of the stellar image parameters. However, the nature of Gaia's observations (TDI and windowed - only a small region around the image or spectrum is read out from the CCD and telemetered to the ground) means that radiation damage also induces signal loss. This signal loss is expected to degrade the predicted scientific performance of the mission. In Chapter 3, for CCDs with a fully functioning SBC, we predict a performance degradation of about 10% (over the CTI-free case). With missing SBCs this performance loss will be higher.
Gaia's CCDs have already been integrated on to the satellite and so it is too late to change which CCDs are selected to fly on Gaia. Nevertheless, the enormous amounts of data that Gaia will produce in its 5-year mission means it is important to establish, as much as possible before the mission starts, the potential impact on the mission of missing SBCs. This chapter addresses the following issues:

1. Whether SBCs were working properly in Gaia CCDs used to predict the mission performances and against which mitigation models are being developed and tested.
2. In the absence of testing whether FM CCDs have functional SBCs as a criterion for selecting which CCDs should fly on the Gaia satellite, is it possible to predict how many will have functional SBCs?
3. What is the impact of missing SBCs on the Gaia image location accuracy?

The chapter is organised as follows: the Gaia SBC is introduced in detail in Section 6.2. Section 6.3 reviews measurements of Gaia's SBC in the literature, addressing the first issue listed above. The next three main sections each present new results on whether SBCs are working or not in Gaia's CCDs: re-analysis of existing data (Sections 6.4 and 6.6) and new data obtained and analysed for this chapter (Section 6.5).
Section 6.4 re-analyses the Hopkinson (2006) data set, which includes SBC measurements of seven Gaia CCDs and identifies a probable new case of non-functional SBCs (Section 6.4.2). This case is subsequently modelled (Section 6.4.3) to investigate whether the measurements can be interpreted as evidence for non-functional SBCs, which is discussed in Section 6.4.5. The next main section (Section 6.5) presents new pocket pumping measurements and analysis of a Gaia CCD test structure. The final main section (Section 6.6) presents a re-intepretation of data obtained from irradiated devices

tested by EADS-Astrium, the Gaia main industrial partner, in terms of SBC efficiency, which addresses the first issue raised above.
Section 6.7.1 addresses the second issue raised above by tentatively predicting how many CCDs on the Gaia satellite will have fully functional SBCs. The third issue raised above is addressed by repeating the detailed characterization of the impact of CTI effects on the Gaia image location accuracy of Chapter 3, using synthetic data for which a non-functional SBC has been simulated. We conclude in Section 6.8 before presenting specific recommendations for future testing for SBC efficiency in Section 6.9, both pre-launch on-ground testing and post-launch in-flight testing.

6.2 The Gaia CCD pixel architecture

A modern CCD has an electrode structure with transfer channels or columns formed by implanted doping in the underlying silicon (see Fig. 6.1). The structure is termed Buried Channel (BC) because the design is such that the charge signals are collected and subsequently transferred within the silicon and away from the silicon/silicon dioxide interface states (the layer between the silicon and the electrodes). A pixel with only a BC and the potential distribution in the pixel in the across-channel direction are shown in Fig. 6.2. The stored charge generally occupies the whole width of the channel. However, by including a narrow region of additional channel doping (in Gaia's case at one side), as shown in Fig. 6.3, a small deeper potential well is formed and the volume occupied by a small charge signal can be minimised. The additional doping is

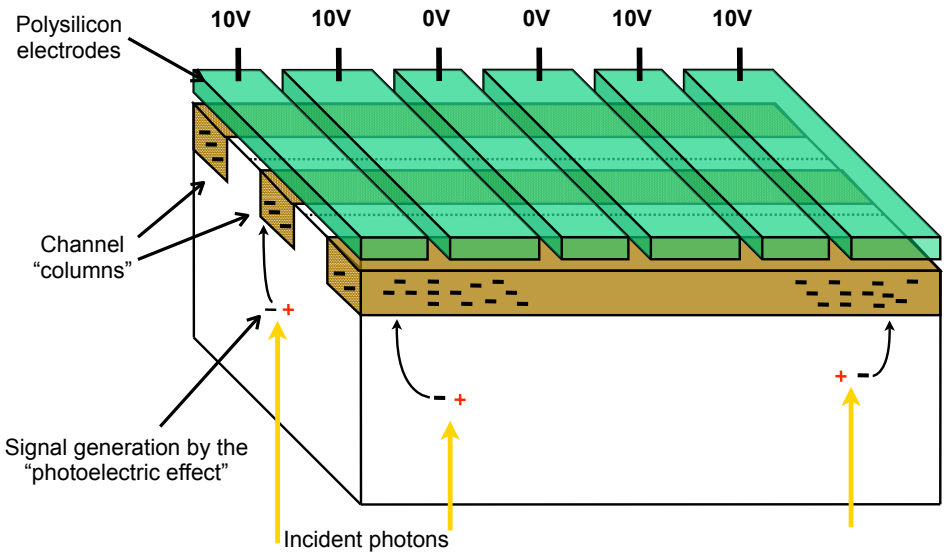

Figure 6.1 — Front-side schematic of a Gaia CCD showing the four-phase electrode structure. Gaia CCDs are back illuminated i.e. incident photons do not pass through the electrodes. Two consecutive electrodes are biased 'high' (10 V), to which photoelectrically generated signal electrons are attracted. Charge packets are separated in the charge transfer direction by biased 'low' (0 V) electrodes. The cube below the electrodes is a block of silicon and the darker regions within the silicon are implanted doping, which form channel columns. Charge packets are separated perpendicular to the charge transfer direction by column isolation regions of undoped silicon.

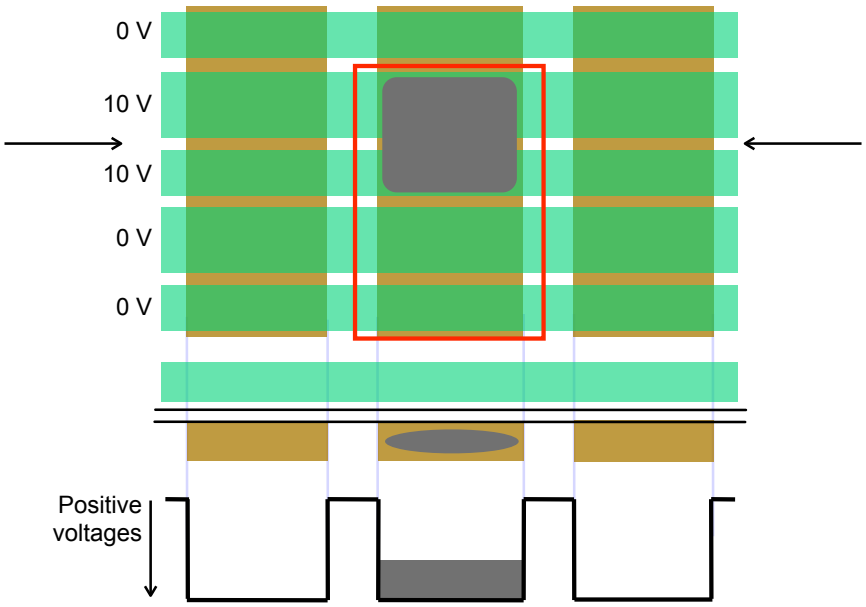

Figure 6.2 — Top: Front-side schematic of a CCD showing BCs with the vertical rectangles, electrodes with the horizontal rectangles, a charge packet in the rounded grey region with a pixel illustrated with a rectangular outline. **Bottom**: Cross-section through the arrows in the above schematic showing a single electrode above three BCs with the charge packet in the middle BC. A simplified potential distribution is below, showing that the charge packet sits within the potential maximum of a BC.

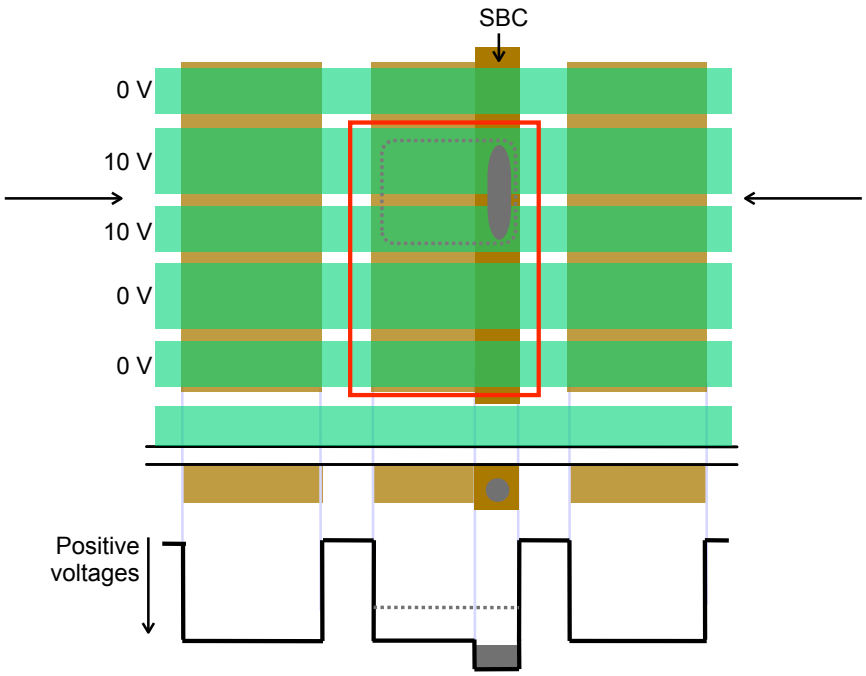

Figure 6.3 — Same as Fig. 6.3 but with SBC doping added to the central BC. The charge packet illustrated is smaller than the SBC capacity and so sits in the SBC volume, rather than the BC volume, (top) and sits in the higher SBC potential maximum, rather than the lower BC potential maximum.
Adapted from diagrams courtesy of D. Burt. (e2v technologies)

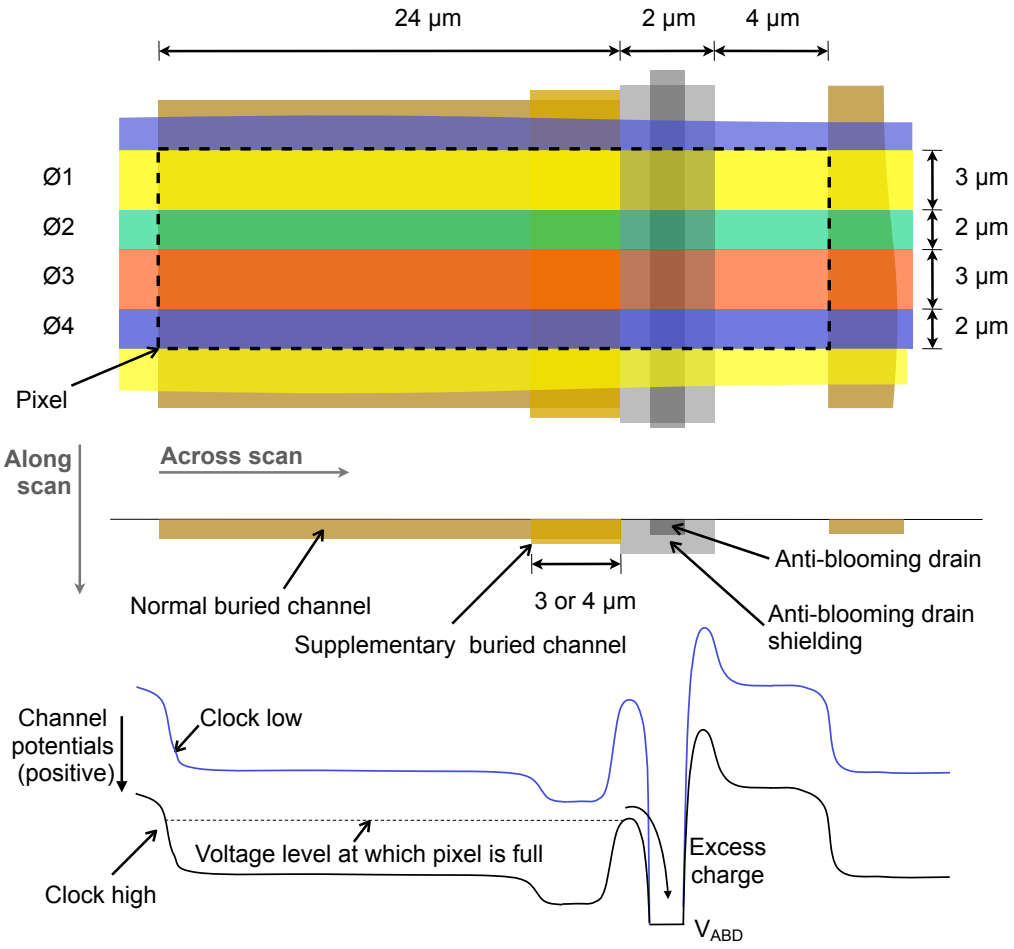

Figure 6.4 — Detailed schematic of the Gaia CCD pixel architecture. *Top*: Front-side schematic of a Gaia CCD pixel showing the four electrodes (ϕ) with pixel features labelled. *Middle*: Schematic of the vertical cross-section through the top schematic in the across-scan direction. *Bottom*: Channel potential profile in the same direction, resulting from different voltages being applied to the electrode (clock low $= 0$ V, clock high $= 10$ V). Diagram courtesy of D. Burt (e2v technologies)

termed a SBC or 'notch'. Once the capacity of the SBC is reached, any further charge spreads out to cover the whole BC volume, as shown dotted in Fig. 6.3.

The CCD91-72 was designed and manufactured by e2v especially for Gaia. Gaia has one of most complex pixel architectures built for astronomy (see Fig. 6.4). It includes the standard BC, the relatively rare SBC and, unusually, an Anti-Blooming Drain (ABD). Gaia is the only astronomical detector with an ABD. It prevents charge bleeding down columns from bright observations, allowing simultaneous faint observations. The ABD also removes excess charge from just upstream of TDI gates. These gates located at different positions within each CCD block charge packets of very bright observations that would otherwise saturate the pixels. This allows their integration to begin just downstream of the TDI gate at shorter distances from the readout register.

The doping that defines each pixel feature is implanted into the CCD silicon using a photo-lithographic mask. Each feature (e.g. BC or SBC) has its own mask. Due to practical manufacturing constraints, the masks are smaller than the image area of

large format devices like the Gaia CCD (4.5 cm $\times$ 5.9 cm). As only one mask can be used at a time, the mask area dictates the area of the CCD that can be implanted with dopant at any one time. This smaller sub-array is called a stitch block (de Bruijne 2008, see Fig. 6.5). Large format devices like the Gaia CCD are fabricated using a photo-lithographic 'step and repeat' process that implants a particular pixel feature simultaneously everywhere in a stitch block, one stitch block at a time. Both Gaia CCD's upper and lower halves are photo-lithographically stitched from 7 repeated stitch blocks and 2 end-termination stitch blocks. A Gaia CCD is thus composed of 18 different stitched blocks. Each termination stitch block contains 108 columns while each repeated stitch block section contains 250 columns: $2 \times 108 + 7 \times 250 = 1966$ columns in the ACross scan (AC) direction and 4500 TDI lines in the ALong scan (AL) direction. The AL direction refers to the travel direction of stars across the Gaia CCDs that is induced by the continuous spinning of the spacecraft around its own axis. And AC refers to the orthogonal direction to this travel direction.

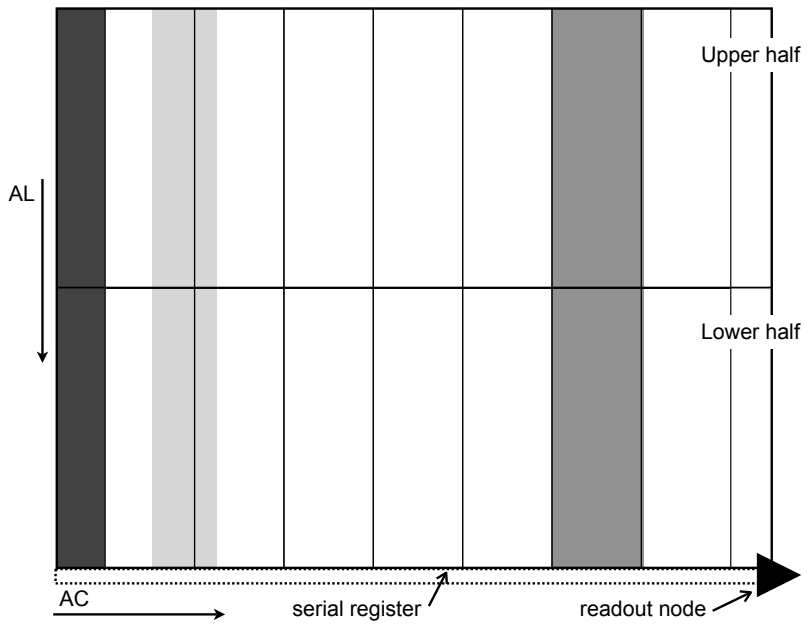

Figure 6.5 — Schematic of the Gaia CCD image area: CCD columns (TDI line ALong scan, AL) are vertical; ACross scan (AC) is horizontal; the readout node is at the bottom right corner. Each rectangle is a stitch block. All the internal lines in the schematic are stitch boundaries. The horizontal stitch boundary is at TDI line 2160 from the serial register (bottom box) and at TDI line 2340 from the start of the CCD (top line in the schematic). We colour-coded three different areas, reference to these areas will be made in the text, from left to right: (i) the dark grey (rightmost) area covers columns 359-608, corresponding to two stitch blocks in the AL direction (hereafter known as AL stitch block couples), (ii) the medium grey (leftmost) area covers columns 1859-1966, which corresponds to the AL stitch block couple identified as a candidate for missing SBCs in the Gaia CCD EM 03153-20-01. (iii) the light grey (central) area covers columns 1550-1755, which corresponds to the area over which the 05256-17-02 CCD was irradiated.

6.3 The SBC Full Well Capacity issue

All the Gaia CCDs (DMs, EMs and FMs) were built from the same nominal pixel architecture design, including SBCs. Therefore measuring the SBC FWC in as many of these devices as possible constrains the expected manufacturing spread of SBC FWCs. In the following we give a summary of the different measurements that have been carried out on irradiated CCDs (Section 6.3.1) and non-irradiated devices (Section 6.3.2). As a result this section is also a summary of the different methods that can be used to measure the SBC FWC and test the functionality of a SBC.

6.3.1 Measurements on irradiated CCDs

First Pixel Response:
The first published estimate of Gaia's SBC FWC was estimated from First Pixel Response (FPR, see Section 6.4.1 for details) measurements made on a Gaia EM CCD (Hopkinson et al. 2005). In their Fig. 11 Hopkinson et al. (2005) show FPR data from columns close to the readout node (although the column numbers are not specified). In Fig. 6.6 we reproduce the same results but only including measurements taken in columns 359-608 (the dark grey area in Fig. 6.5). This range of columns corresponds to two stitch blocks in the AL direction (hereafter known as AL stitch block couples). Hopkinson et al. (2005) estimated the SBC FWC to be $\sim$1400 e^-. However, this is a typographical error in their paper. The arrow defining their SBC FWC in their Fig. 11 is pointing to $\sim$1400 ADU, which corresponds to $\sim$1100 e^-. Fig. 6.6 shows that this signal level corresponds to the first inflexion point. It is at this signal level that the number of electrons in the SBC start to collapse the SBC potential so some of these electrons spill out of the SBC potential into the BC potential. No longer protected in the smaller volume of the SBC, these few electrons in the BC meet more traps, causing the fractional charge loss increase. At the second inflexion point, the signal level has completely collapsed the SBC potential into the BC potential so here the SBC no longer exists and all the electrons sit in the BC potential. Fig. 6.6 shows that without SBCs in each column, the BC fractional charge loss would continue to increase as signal level decreases. In other words, the presence of SBCs causes the fractional charge loss curve to shift left to smaller signal levels so that at a given signal level the fractional charge loss in the SBCs is less than in the BCs.
On its own, Fig. 6.6 only demonstrates that the stitch blocks from which the data was obtained have working SBCs. Because of the way e2v manufacture the CCDs (all the SBC doping implanted simultaneously, one stitch block at a time), intra-stitch block SBC FWCs should be the same. However, in the Gaia case, there is no guarantee that inter-stitch block SBC FWCs will be the same. This is due to the SBC doping abutting the Anti-Blooming Drain (ABD) doping (see Fig. 6.4 top schematic) and overlapping the ABD shielding doping (see Fig. 6.4 middle schematic). The ABD doping is the first pixel feature to be implanted into each pixel within a stitch block area of CCD silicon using its own photo-lithographic mask (the size of a stitch block). The ABD mask is aligned to the 'zero grid'. All the SBCs in the same stitch block have their doping implanted subsequently using a SBC photo-lithographic mask aligned to the same zero grid. Each mask alignment to the zero grid is subject to random alignment

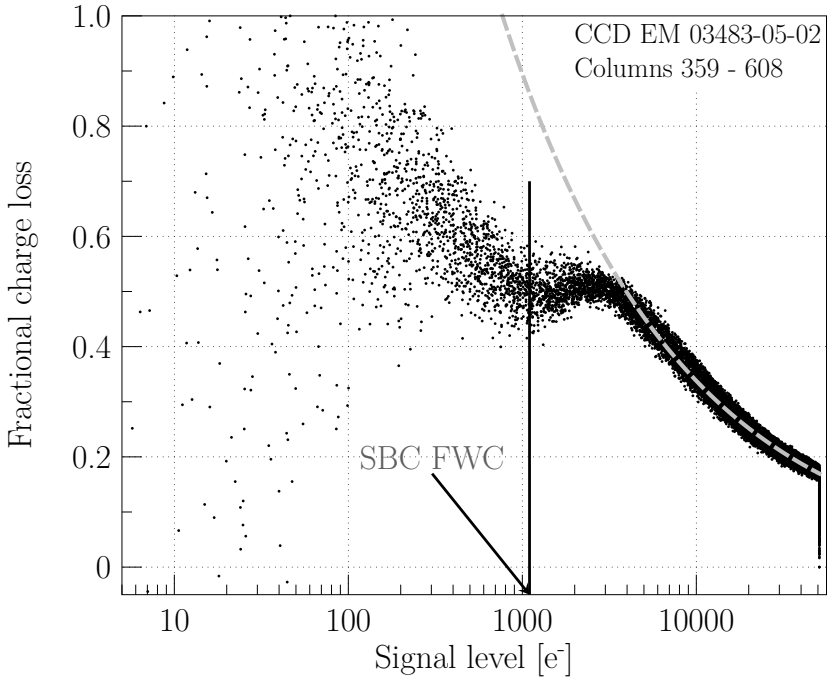

Figure 6.6 — First Pixel Response (FPR, see Section 6.4.1 for details) measurements made on a Gaia EM CCD: fractional charge lost due to radiation damage as a function of signal. In this case, the SBC FWC is evaluated to be ∼1100 e^- (black vertical line) following the definition of Hopkinson et al. (2005). In grey (dashed line), a power law is fitted to the fractional charge loss in the BC regime (signal level > 3500 e^-). The extrapolation of this fit in the SBC regime (signal level < 3500 e^-) shows the expected fractional charge loss for a CCD containing no SBCs.

(stitch) errors of $\leq$0.25 μm (Burt 2005a). Because the ABD shielding doping cancels out the SBC doping, the effective SBC doping width, consequent potential depth and resulting FWC is sensitive to the stitch error. Therefore, scatter in inter-stitch block SBC FWC (both intra-CCD and inter-CCD) is expected from the nominal e2v design of the Gaia CCDs.

The second published measurement of Gaia's SBC FWC can be read off from Fig. 5 in Chapter 2, which shows the fractional charge loss as a function of signal level for a different Gaia CCD, irradiated and tested by the prime contractor for Gaia EADS-Astrium in their second Radiation Campaign (RC2). This chapter reproduces the results of Chapter 2 in Fig. 6.10 (right). Following the SBC FWC definition of Hopkinson et al. (2005), the read off value is ~ 500 electrons. Note that the CCDs referred to in Hopkinson et al. (2005) and Chapter 2 were irradiated at different doses (respectively 1×10^{10} and 4×10^9 protons cm^{-2} 10 MeV equivalence), as seen by the different amplitudes of the fractional charge loss in their figures. Yet both CCDs exhibit the clear break in the increase of the fractional charge loss as the signal level decreases. This can only be explained by the presence of SBCs. While Hopkinson et al. (2005) fractional charge loss values are derived from different levels of uniform charge injections (CIs), Chapter 2 values are derived from one non-uniform CI. This means that the different data points in Chapter 2 come from different AL stitch block couples. The small scatter in their results indicates that the tested CCD has similar SBC FWCs in each of its AL

stitch block couples. This is important to establish as this CCD was used to establish the efficiency of CI as a CTI mitigation tool. RC2 data was since been used to further investigate CI and for verification of CTI modelling Chapter 2. Therefore all results based on this RC2 CCD are representative of the scenario where all Gaia CCD stitch blocks have working SBCs.
In the CCD upper half (cf. Fig. 6.5) the nominal SBC doping width is 3 μm, whereas in the CCD lower half the nominal SBC doping width is 4 μm (Burt 2003). This is because every CCD column and so every SBC crosses the horizontal stitch boundary. The SBC doping width is increased immediately after the stitch boundary to minimise the possibility of the SBC narrowing at the boundary as it is known that boundaries can cause the formation of a potential pocket, which acts like radiation traps, capturing and then releasing electrons and thus increasing CTI. This difference between the nominal SBC doping widths in the upper and lower halves of each Gaia CCD translates to different SBC FWCs in either half. All FPR data passes through both halves of the CCD so the fractional charge loss is the total over the entire column. Charge packets larger than the SBC FWC of the upper half and larger than the SBC FWC of the lower half will traverse the entire column in the BC. Charge packets smaller than the SBC FWC of the upper half will also be smaller than the SBC FWC of the lower half and so will traverse the entire column within the SBC. Charge packets larger than the SBC FWC of the upper half but smaller than the SBC FWC of the lower half will traverse the upper half of the column in the BC and the lower half within the SBC. In this case, the fractional charge loss will be greater than if the SBC doping width was 4 μm in both halves but less than the fractional charge loss if the SBC doping width was 3 μm in both halves. Therefore, the first inflexion point in Fig. 6.6 represents an average SBC FWC over the two halves of the CCD.

6.3.2 Measurements on non-irradiated CCDs

Pocket Pumping:
Unlike the FPR technique, pocket pumping can provide an independent measure of the SBC FWC in each half of a CCD. Charges from a flat field illumination are moved back and forth in the image area over a one pixel length. In pixels with traps, single electrons can be statistically trapped during one half-cycle and then released during the next half-cycle into the adjacent pixel. This produces bright-dark pairs around the mean flat field level at the trap position. Repeating the technique with increasing mean flat field signal levels identifies the number of traps per pixel as a function of signal size. This method was used by Kohley et al. (2009) to determine the number of fabrication-induced single electron traps in each pixel of a non-irradiated Gaia FM CCD. Their Fig. 9 shows that the SBC FWC (averaged over all the pixels in a stitch block) in each stitch block in the upper half of that CCD was measured to be less than 40 e^-. For a SBC FWC < 40 e^-, the depth of the SBC potential is very likely to be of the order of the thermal voltage, making thermal electron diffusion out of the SBC into the BC highly probable. In this case case the SBC is in practice absent. The SBC FWC (averaged over all the pixels in a stitch block) in each stitch block in the lower half of that CCD was measured to range from 1000 to 3000 e^-. Their Fig. 9 shows that they used the first inflexion point definition of SBC FWC. Kohley et al. (2009) is the first

published evidence that there is an issue with the Gaia SBCs. This chapter re-analyses the Hopkinson (2006) data set, which includes the Hopkinson et al. (2005) Gaia CCD as well as six others, to see how common working SBCs are in the upper halves of Gaia CCDs.

e2v's analytical Gaia CCD design predictions (published for the first time in Seabroke et al. 2010) are actually an order of magnitude higher than the SBC FWCs reviewed in this section: 7900 e^- in the upper half and $13\,000$ e^- in the lower half. Seabroke et al. (2010) provided an explanation for the discrepancy between these predicted and measured FWCs: none of the Gaia CCDs measured so far seem to have the nominal SBC doping widths. This explanation was investigated by simulating smaller SBC doping widths in a 3D semi-conductor physics model of the Gaia pixel. Seabroke et al. (2010) Fig. 5 shows that the simulated SBC FWCs agree with the Kohley et al. (2009) measured FWCs when the simulated SBC doping widths are $\leq$1.5 and 2 μm for the upper and lower halves of the CCD respectively. The resulting potential profiles in the $\leq$1.5 μm simulation showed no evidence for a SBC, only a BC. These simulated SBC doping widths are systematically 2 μm smaller than the nominal widths in both CCD halves. Worst-case random alignment stitch errors (-0.5 μm) applied to the nominal SBC doping widths cannot explain the offsets. The range of SBC FWCs in the lower half of the CCD measured by Kohley et al. (2009) agree with the simulated FWCs taking into account the worst-case random stitch error between two pixel features within a stitch block being $\pm$0.25 μm. Therefore these offsets appear to be uncalibrated systematic offsets in e2v photo-lithography, which could either be due to systematic stitch offsets or lateral ABD shield doping diffusion. The Seabroke et al. (2010) pixel model does not specifically simulate either of these scenarios, rather it simulates the same effective SBC doping width that could be produced by both or either of these scenarios.

Minimum Injection Method:

Figs. 6.7 and 6.8 illustrate different CI methods available on the Gaia CCDs: (top) the Voltage-Tunable Method (VTM) and (bottom) the Minimum Injection Method (MIM). The horizontal lines under the Injection Diode (ID), Injection Gate (IG) and electrodes (Iϕ1, Iϕ2 and Iϕ3) are representative of the voltage applied to each. Like in Figs. 6.2, 6.3 and 6.4, the convention of plotting low voltages levels as upper horizontal lines and high voltage levels as lower horizontal lines allows the voltage levels to also represent potential levels with electrons filling them up (grey regions) from the bottom (higher voltage) to the top (lower voltage), analogous to water filling up a bath. The top schematic in Fig. 6.7 shows the IG with a voltage level lower than ID and Iϕ1 so electrons (like bathwater) cannot flow from ID to Iϕ1. The ID fills up with electrons and the middle left schematic shows that when the level of electrons is higher than the IG, they can flow to Iϕ1. The bottom schematic in Fig. 6.7 shows the ID no longer filling up with electrons. This stops the flow of electrons across the IG, leaving electrons now occupying both the ID and Iϕ1. The voltages that are tunable in the VTM are IG and Iϕ1 (see the equation in Fig. 6.7).

The idea behind MIM is to transfer charge into Iϕ1 without the amount of charge stored in Iϕ1 depending on the voltages applied to IG or Iϕ1. This can be achieved by having

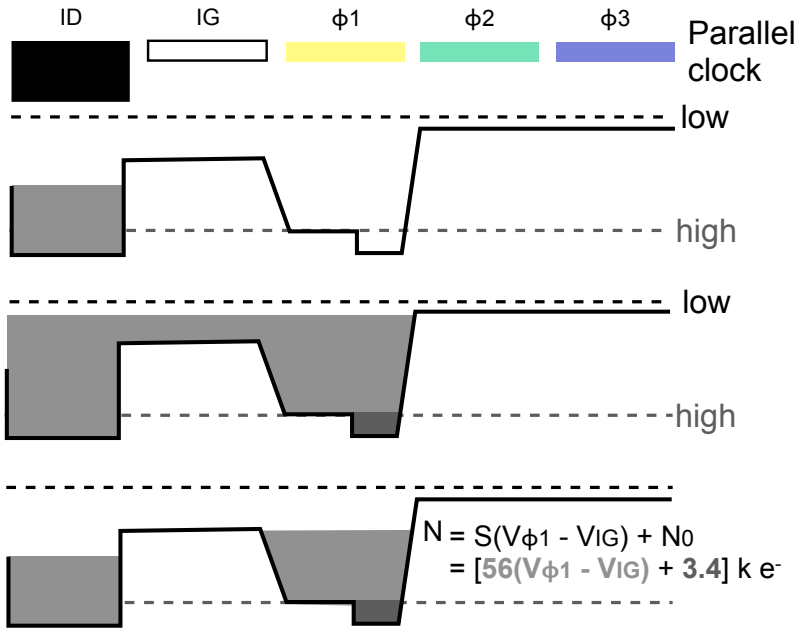

Figure 6.7 — Voltage-tunable method, where the quantity of charge depends on the difference of voltage between the 'high' level of the image section clock Iϕ1 and that on IG (Injection Gate). Note that the width of ID (Injection Diode) and IG are only schematic and so actually differ from one another. Also only 3 out of the 4 electrodes contained in a Gaia CCD pixel are depicted. Figure adapted from Burt (2003) Fig. 3 (i) and labelled with the latest e2v predicted levels of injected charge from Burt (2005b).

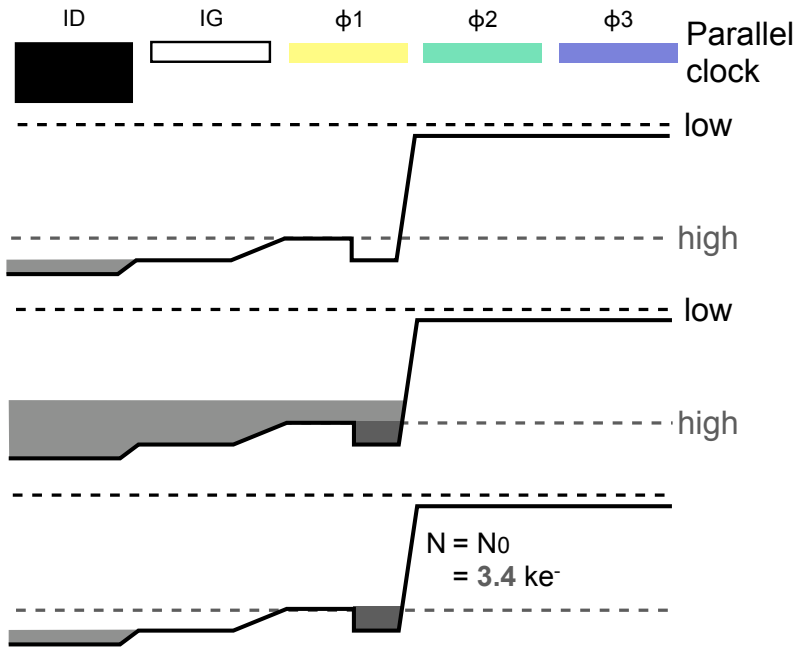

Figure 6.8 — Minimum injection method, where the quantity of charge is independent of the difference of voltage between the 'high' level of the image section clock Iϕ1 and that on IG and only depends on the SBC capacity under Iϕ1 (N_0). Note that we did not depict the case for which Iϕ2 is also biased high, such that electrons are also injected under Iϕ2.

ID > IG > Iϕ1 (see top schematic in Fig. 6.8). When the ID fills ups with electrons they can flow across the IG into Iϕ1 (see middle schematic in Fig. 6.8). As with the VTM, when the ID no longer fills up with electrons, the flow of electrons across the IG is stopped. As the electrons are attracted to the highest voltage, they drain back across IG to ID. However, because there is a SBC under Iϕ1 and its voltage is higher than Iϕ1, the electrons filling the SBC remain there and only the excess electrons drain out of Iϕ1. In theory MIM enables the precise injection of a very low level of charge independently of the voltage settings. The SBC FWC should be more reproducible column-to-column than using only the difference of voltage between the 'high' level of Iϕ1 and that on IG to inject the same small amount of charge. Without a SBC under Iϕ1, the equations in Fig 6.7 show that to inject 3400 e^- requires 0.06 V. Variations in oxide charge from pixel to pixel cause small fixed voltage offsets between columns at this level, which means that a single applied voltage to a single gate results in a non-uniform distribution of potential column-to-column and thus a non-uniform distribution of injected charge column-to-column. e2v expected MIM to have higher CI uniformity than VTM but this assumes only a small scatter in SBC FWCs. As explained in Section 6.2, SBC FWC should be uniform within a stitch block but can vary between stitch blocks. Therefore, MIM may only have higher CI uniformity than VTM within a stitch block but not necessarily over an entire CCD.
The original layout (pre-2004) of the CI structure included Iϕ1 with the nominal AL dimension of 3 μm and an underlying SBC foreshortened in AL by 1 μm (i.e. 3 $\times$ 2 μm). Burt (2005b) reports that e2v MIM testing of this structure did not find N_0: the electron capacity under Iϕ1 (see Fig. 6.8). This was because the SBC potential was not there as its electrical size was smaller than the geometrical size due to fringing fields and manufacturing tolerances. Therefore, the CI structure was modified such that Iϕ1's AL dimension was extended to 5 μm and the SBC increased in size to 3 $\times$ 3 μm to reduce fringing fields and increase the SBC FWC under Iϕ1 only. However, MIM testing of this new CI structure on a few devices still did not find N_0 (T. Eaton, e2v, private communication). This suggests that the post-2004 CCDs tested by e2v do not have working SBCs in their upper halves like the post-2004 CCD measured by Kohley et al. (2009). MIM testing was first suggested by Holland & Smith (2004) to investigate continuous CI. Now, MIM testing is an option for all Gaia FMs during in-flight commissioning to determine whether the FMs have working SBCs in their upper halves.

6.4 FPR measurements: Model to Data comparison

In this section we apply the First Pixel Response technique to laboratory measurements collected from irradiated Gaia CCDs. We then analyze the obtained results by using a detailed Monte Carlo simulation. This analysis is subsequently used to assess what fraction of the CCDs (or AL stitch block couples) are affected by the SBC issue.

6.4.1 Principles of the FPR measurement

Before explaining the details of the First Pixel Response measurements we first briefly review the physical process of electron trapping due to radiation damage. Non-ionising

displacement damage occurs when sufficiently energetic protons knock silicon atoms out of their lattice positions across the entire CCD. The resulting vacancies can move around the lattice until they combine with other atoms, e.g. phosphorous or oxygen, or combine with other vacancies in the BC and SBC to form electron traps, with different discrete energy levels between the valence and conduction bands.
Following the Shockley-Read-Hall formalism (Shockley & Read 1952; Hall 1952) that describes the capture and release of a charge by a trap as decay process, one can derive the capture and release probabilities (for a detailed derivation see Chapter 2). The probability that an empty trap captures an electron within a time interval t is:

$$p_{\mathrm{c}}(t) = 1 - e^{-r_{\mathrm{c}}t}\,, \tag{6.1}$$

$$r_{\mathrm{c}} = \frac{1}{\tau_{\mathrm{c}}} = \sigma_{\mathrm{t}} v_{\mathrm{th}} n_{\mathrm{e}}\,, \tag{6.2}$$

where r_{c} is the capture rate, τ_{c} the capture time constant, σ_{t} the capture cross section, v_{th} the electron thermal velocity, and n_{e} the electron density at the trap location. As a consequence the charge loss that is driven by the capture of charges is particularly sensitive to the electron density. The electron density distribution is shaped by the pixel architecture: as already mentioned, for high signal levels the electron packets sit in the BC and for low signal level in the SBC. The SBC confines the charge packet to a smaller volume and thus affects the electron distribution and the charge loss. Hence studying the charge loss and in particular the fractional charge loss allows us to probe the electron density and characterize the SBC.
The FPR measurement consists of the analysis of the charge loss (induced by trapping) that occurs in the first pixels of a well-characterized signal after its transfer across the full CCD image area. By well-characterized signal, we mean a signal for which the shape and the number of charges is known independently from the CTI effects.
As already explained, on top of the 4 electrodes required to transfer the charges from one pixel to its neighbour, in the first row only, the Gaia CCD pixels comprise a diode to generate artificial charges and a gate to control the number of artificial charges injected i.e. effectively transferred across the CCD (see Figs. 6.7 and 6.8). During the Gaia mission, CIs will be performed periodically (every ~ 1 s) by blocks of 4 to 20 lines to fill a large fraction of the traps prior to the stellar transits and thus mitigate the CTI effects.
CIs are particularly suitable to perform a FPR measurement. In a CI block of several tens of lines, the first line undergoes the most damage by encountering a certain fraction of the total amount of active traps (i.e. the empty traps) present in the signal confinement volume. As we shall see this fraction depends on the CI level (the number of electrons per pixel in the CI block) and the electron density distribution within a pixel. Depending on the capture cross-section of the trap species present and the clocking rate, the first CI line may not fill all the encountered traps. In this case the second CI line will also experience charge loss and subsequently for the other lines of the CI block. After a certain number of lines, no significant trapping can be measured. Using the last lines of a CI block one can measure a reference CI level, N_{ref}, and thus compute the charge loss Δ (i.e. the total number of trapped charges), and the fractional charge

loss δ:

$$\Delta = \sum_{i=0}^{S-1} N_{\text{ref}} - N_i \,, \tag{6.3}$$

$$\delta = \frac{\Delta}{S\, N_{\text{ref}}} \,, \tag{6.4}$$

where N_i is the number of e^- pixel^{-1} in the i^{th} line of the CI block. The traps filled by the CI with a release time constant shorter than the CI block duration will release electrons within the CI block and can thus bias the measurement of the CI reference level. To minimize this source of uncertainty only the first lines of the CI block should be considered in the charge loss measurement. The charge loss measured in the first lines of a CI block depends on the state of the traps at the time they are encountered by the CI signal. The trap state is set by the CCD illumination history. During a FPR experiment, it is thus important to have a good control (or at least a good knowledge) of the CCD illumination history. In the FPR experiments carried out by Hopkinson et al. (2005) to characterize the effect of the SBC, two CI blocks were performed with 100 lines of delay between them. The first CI block was performed to reset the illumination history, and only the second block was used to measure the charge loss. The level of the first block was fixed to $30\,000$ e^-, while the level of the second block was varied. In this way, one can study the charge loss variation as a function of signal level which enables the characterization of the notch architecture within a CCD pixel column. Although information from the CI will be available during the mission, it is not foreseen (at least during operational phase) to vary the CI level. This means that only very limited FPR information will be available (the minimum injection method discussed in Section 6.3.2 will likely only be used during the Gaia commissioning phase, if at all).

6.4.2 Selection of the experimental data

The Sira electro-optics tests were carried out on seven Gaia Astrometric Field (AF) DM and EM CCDs (see Table 6.1). Two of them were front-illuminated CCDs and the rest back-illuminated. This was the first set of CCD radiation test data obtained by an industrial partner in the Gaia project. The analyses described in Hopkinson et al. (2005) and Hopkinson (2006) focused on the determination of trap parameters and CCD characterisation. Figures 8-2-2 and 8-2-3 of Hopkinson (2006) show FPR data from different columns from different AL stitch block couples but not all groups of columns exhibit the characteristic SBC bump in the fractional charge loss. Here we test the hypothesis that these groups of columns consist of columns from the same stitch block AL couple and search for examples which do not exhibit the characteristic SBC bump in the fractional charge loss. These are candidates for CCDs with missing SBCs. Figure 6.9 shows that only two CCDs out of the seven tested by Sira electro-optics have AL stitch block couples that are candidates for missing SBCs and these only number three AL stitch block couples. It was decided to model the AL stitch block couples that had FPR data extending to the smallest signal levels (EM 03153-20-01 columns 1859–1966, see Fig. 6.5 medium grey area) as this provides more modelling constraints.

Table 6.1 — Summary of the irradiated AF CCDs tested by Sira. The first five digits of the CCD serial number form the batch number. The digits in the batch number refer to when the front-side processing occurred (explained in Section 6.7.1). The first two digits in the batch number are the year e.g. 03 refers to 2003. The second two digits in the batch number are the week of the year e.g. 15 out of 52. The fifth digit in the batch number is the number of batches in that week e.g. 3rd batch of week 15 in 2003. The middle set of two digits in the serial number gives the wafer number. The other set of two digits refers to the position of the CCD within the wafer.

Serial Number	Model (Extra information)
03153-05-02	DM (front illuminated)
03153-07-01	DM (front illuminated)
03153-16-02	DM
03153-20-01	DM
03442-11-01	EM
03483-05-02	EM
03483-06-02	EM

6.4.3 Generation of the synthetic data

In order to reproduce the FPR measurements, we simulate the transfer of a CI block over the image area of a virtual irradiated CCD using the detailed Monte Carlo model of charge transfer presented in Chapter 2[1]. This model was verified against experimental data acquired with Gaia irradiated CCDs. In particular, by using a flexible and analytical representation of the electron density distribution, the model is able to accurately reproduce the measurement of fractional charge loss as a function of signal level in the presence of an operational SBC (in both CCD halves). In the following we first describe the used electron density distribution model (Section 6.4.3.1). Then we present the simulation setup (Section 6.4.3.2) and the comparison procedure (Section 6.4.3.3) we used to reproduce the selected experimental data.

6.4.3.1 Modelling the electron density distribution

In the CTI effects model we used, electron packets are transferred at the pixel-electrode level and the trapping processes are simulated by computing the probabilities of the electron capture and release at the level of each individual trap. This necessitates the modelling of the electron density distribution n_{e} at the location $\mathbf{x} = (x, y, z)$ of each trap in the pixel signal confinement volume V. The latter corresponds to the volume occupied by an electron packet at the pixel FWC ($\sim 190\,000\ \mathrm{e}^-$ for a Gaia CCD). It is assumed to be a box for which the dimensions are set by the manufacturing characteristics of the CCD.

The electron density distribution is analytically described by a normalized Gaussian function in the three space directions. To take into account the effect of the SBC on the electron density distribution at low signal level, the distinction between two signal regimes is made and a smooth transition between these regimes is ensured:

$$n_{\mathrm{e}}(x, y, z) = S \times \rho(x, y, z) = S \times \rho(\mathbf{x})\,, \tag{6.5}$$

1. This model can be used as part of the Java package CEMGA available online `http://www.strw.leidenuniv.nl/prodhomme/cemga.php`

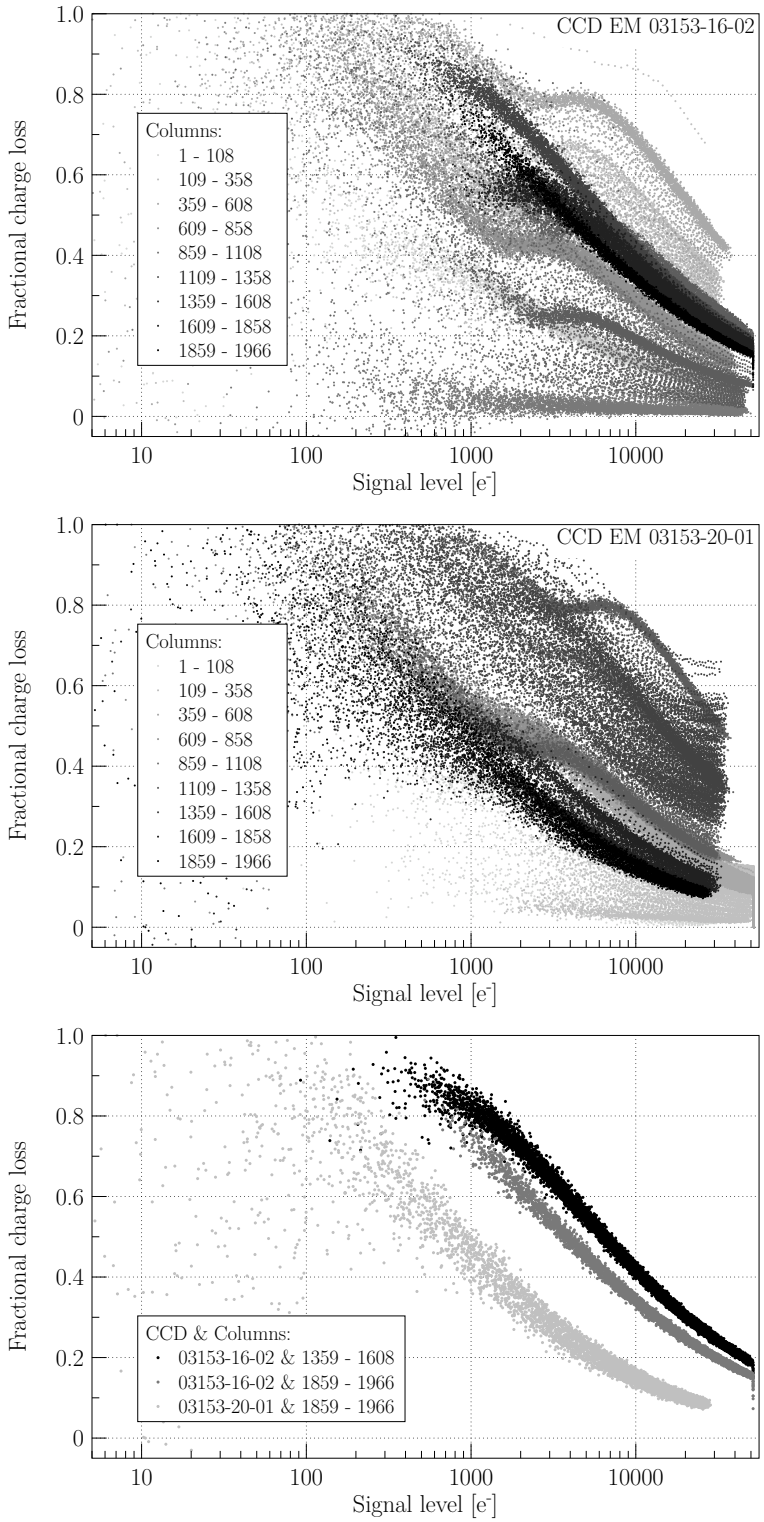

Figure 6.9 — Top and middle: FPR plots of the two CCDs out of the seven including AL stitch block couples that are candidates for missing SBCs. **Bottom:** FPR plots of the three AL stitch block couples that are candidates for missing SBCs.

$$\rho(\mathbf{x}) = \frac{\exp\left[-\frac{1}{2}\left(\left(\frac{x-x_0}{\sigma_x}\right)^2 + \left(\frac{y-y_0^\star}{\sigma_y^\star}\right)^2 + \left(\frac{z-z_0^\star}{\sigma_z^\star}\right)^2\right)\right]}{\left(\sqrt{2\pi}\right)^3 \sigma_x \sigma_y^\star \sigma_z^\star}\,, \tag{6.6}$$

where S is the signal level, and x, y, z respectively the CCD parallel and serial transfer direction, and depth. $\sigma_{\mathbf{x}}$ and $\mathbf{x}_0$ are the distribution standard width and centre coordinates along these directions. The parameters indicated with a $\star$ vary as a function of signal level:

$$P^\star = P_{\text{BC}}\left(1 - e^{-\frac{S}{S_{\text{BC}}}}\right) + P_{\text{SBC}} e^{-\frac{S}{S_{\text{SBC}}}}\,, \tag{6.7}$$

where P_{BC} refers to the parameter value in the BC and P_{SBC} to the corresponding value in the SBC. As already mentioned the SBC confines the electron packet in depth (z) and in the serial transfer direction (y), but the packet remains spread under two electrodes in the parallel transfer direction (x) independently of the signal regime. Thus, in the model, the SBC and BC signal confinement volumes have different dimensions along y and z ($y^\star_{\text{max}}$, $z^\star_{\text{max}}$), but the same size along x (x_{max}). Accordingly the centre and the standard widths of the density distribution along y and z are different for the BC and SBC regimes. For each regime, the distribution standard width in one direction is set to a fraction η of the signal confinement volume dimension in that direction, e.g.:

$$\sigma_y^\star = \eta^\star \times y^\star_{\text{max}}\,. \tag{6.8}$$

In this way the ratio between the dimensions of the signal confinement box is preserved in the electron density distribution. The greater is η the more spread is the electron distribution. η is thus later referred to as the electron density distribution spread factor. Saturation occurs at high signal close to FWC_{BC} and the modelling of this process is described in Chapter 2. The transition between the two signal regimes occurs at S_{SBC}. It is important to note that although in reality S_{SBC} would be compared to the FWC_{SBC}, in the presented model, due to the arbitrary nature of the chosen description for the transition between the BC and SBC regimes, S_{SBC} does not carry any real physical meaning.

6.4.3.2 Simulation setup

During the experiments carried out by Hopkinson, two CI blocks were transferred. The first CI block was used to reset the illumination history by filling a large fraction of the empty traps. The second block was used to perform the FPR measurement and its level varied. For most of the tested levels, the level of the first block ($\sim 30\,000$ e^- pixel^{-1}) was higher than the level of the second. As a consequence the population of traps probed by the second CI block was the same as for the first. However from this population the only traps capable of capturing electrons from the second block, are by definition the empty traps: the ones that were able to release their electron before the crossing of the second block. In our simulated experiment we can thus simulate the transfer of a unique CI block (of 50 lines) crossing the image area of a CCD containing only empty traps and perform the FPR measurement on this very same CI block. As for this particular experiment we are interested in the electron capture only, we used a unique

trap species with a common capture cross section ($\sigma_t = 5\times10^{-15}$ cm^2) and a long release time constant compared to the duration of the CI (50 $\times$ 0.9892 ms) such that the charge loss and the reference level measurements are not biased by a significant release of electrons. The simulated CCD image area consists in a single column of 4500 pixels. We did not simulate the transfer across the serial register, as one can to first order ignore the effects of the serial CTI. In order to investigate the potential difference of SBC implant between the first and second halves of the CCD, the standard widths of the electron distribution in the SBC regime and S_{SBC}, the SBC to BC regime transition signal, can be set to different values for the two CCD halves:

$$\eta_1^\star \leq \eta_2^\star\,, \tag{6.9}$$

$$S_{SBC_1} \leq S_{SBC_2}\,. \tag{6.10}$$

The BC and SBC signal confinement volumes as well as the standard widths of the electron density distribution in the BC regime remain the same for the two CCD halves. Note that the parameter label 1 refers to the CCD upper half i.e. the furthest away from the serial register. Once the CI block is transferred through the two CCD halves, the FPR measurement is performed in the same way as for the experimental test (Section 6.4.1). For each set of simulation parameters, the CI level is varied from 50 to 40 000 e$^-$ (with 200, 500, 2 000, 5 000, 20 000 e$^-$ as intermediate values).

6.4.3.3 Model to data comparison

In our simulations, there are 7 free parameters:

1. η_{BC}, η_1 and η_2 the electron density distribution spread factors, that set the standard widths of the electron distribution for each signal regime and CCD half according to the signal confinement volume dimensions,
2. S_{SBC_1} and S_{SBC_2} the signal level at which the transitions between the SBC and BC regimes is performed,
3. N_t the number of traps per pixel.

Table 6.2 details all the simulation parameters and indicates the values we used for the fixed parameters as well as the allowed intervals for the free parameters.
We are not interested in the exact reproduction of the data but rather in the study of the parameters of the electron density distribution model that lead to a reasonable agreement between the simulated and the experimental fractional charge loss measurements over the studied range of CI signal levels. We thus generate random sets of parameters in order to probe homogeneously the entire parameter space. Each parameter set results in a set of data points that sample the simulated fractional charge loss curve. These data points are then compared to the experimental measurements. To proceed to this comparison, we have first generated an analytical representation of the experimental data by the mean of a fit using spline functions. We use the analytical fit values F and the simulation results ϕ at each particular signal level n to compute the χ^2, that constitutes our comparison criterion:

Parameter	Description	Fixed value or [interval]
T	temperature	163 K
P_{TDI}	TDI period	0.9828 ms
N_t	number of traps per pixel	[0–20]
σ_t	capture cross section	5×10^{-20} m^2
τ_r	release time constant	9 s
	BC regime	
η_{BC}	distribution spread factor	[0.05–1]
FWC	BC full well capacity	190 000 e$^-$
	BC signal confinement volume size:	
x_{max}	in the parallel transfer direction	11 μm
y_{max}	in the serial transfer direction	24 μm
z_{max}	in depth	0.75 μm
	SBC regime	
	distribution spread factor:	
η_1	in the CCD upper half	[0.05–1]
η_2	in the CCD lower half	[0.05–1]
	SBC to BC regime transition signal:	
S_{SBC_1}	in the CCD upper half	[1–8000] e$^-$
S_{SBC_2}	in the CCD lower half	[1–8000] e$^-$
	SBC signal confinement volume size:	
$y_{SBC,max}$	in the serial transfer direction	2 μm
$z_{SBC,max}$	in depth	0.1 μm

Table 6.2 — Simulation parameters. Note that we use a non-nominal width for the SBC doping profile in the AC direction: $y_{SBC,max}$ = 2 μm. This value is given by Seabroke et al. (2010) to explain discrepancies between measured and predicted SBC FWC for functional SBCs (see Section 6.3.2).

$$\chi^2 = \sum_{n=0}^{N-1} \frac{\left(\phi\left(n\right) - F\left(n\right)\right)^2}{\sigma^2}\,, \tag{6.11}$$

where N is the total number of simulated CI levels and σ the noise. We use the formal errors associated to the analytical fit to the experimental data as σ values and thus assume that the formal errors encompass the experimental noise and the readout noise.

6.4.4 Comparison results

Figure 6.10 (left) shows the fractional charge loss measurement carried out by Hopkinson (black dots) on the Gaia AF CCD EM 03153-20-01 (columns 1859-1966) along with the result of the presented simulation setup that aimed to reproduce this measurement (red line). The simulation shown is representative of the best fit to the data that can be obtained following a random search in the parameter space. One can first notice a clear deviation at high signal levels ($> 10\,000$ e$^-$). Note that this deviation at high signal levels was already present in an attempt to fit the fractional charge loss

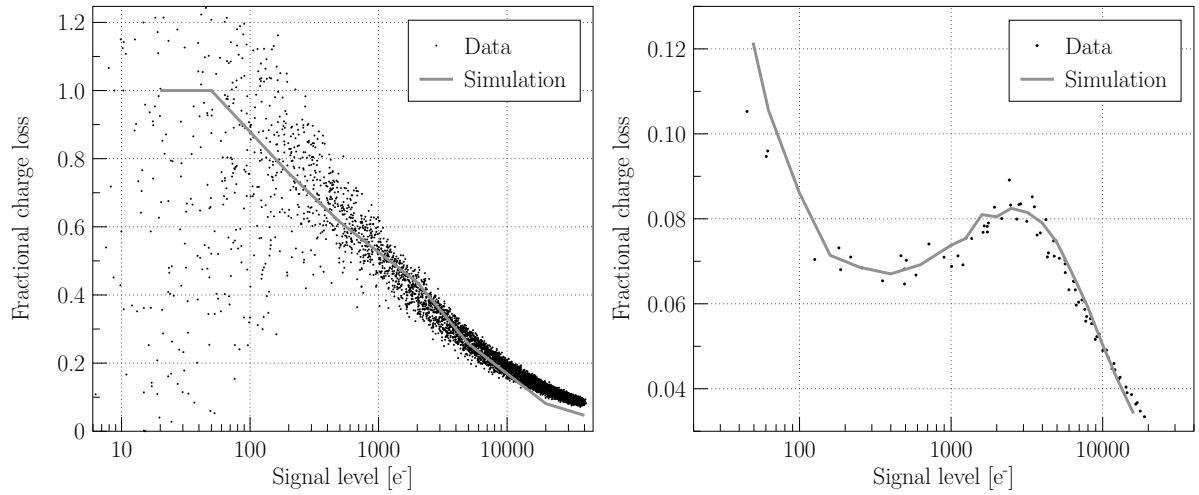

Figure 6.10 — Comparison between experimental (black dots) and simulated (grey line) fractional charge loss measurement as a function of CI level. The left panel shows a subset of Hopkinson's measurements for which the SBC of the CCD upper half is suspected to be not operational. The right panel shows the same measurement extracted from the second campaign of experimental tests carried out by Astrium on an irradiated Gaia CCD that demonstrates the expected behaviour for an operational SBC in both CCD halves. The detailed Monte Carlo model (Chapter 2) in combination with the analytical representation of the electron density distribution is able to qualitatively reproduce the fractional charge loss measurement in both cases.

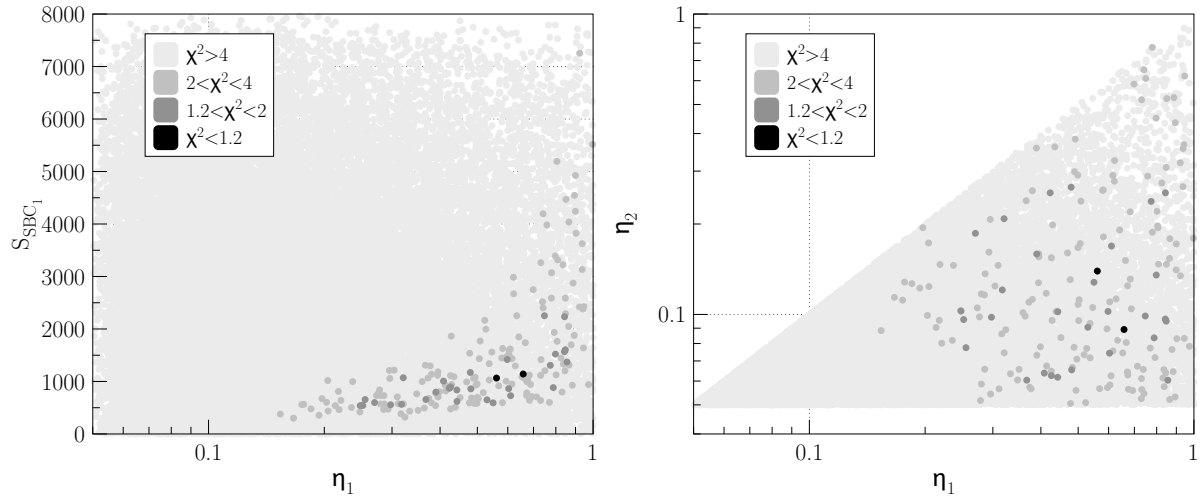

Figure 6.11 — Left: map of the resulting agreement between experimental (Fig. 6.10 left) and simulated fractional charge loss measurements as a function of the free parameters of the simulation for the modelled SBC in first half of the CCD: S_{SBC_1} and η_1. The plotted agreement corresponds to the described χ^2 (see Section 6.4.3.3) normalized by the best χ^2 achieved. This map shows that a reasonable agreement can only be obtained for: either (i) a narrow electron density distribution and a transition between SBC and BC regimes at a low signal level, or (ii) a wide electron density distribution and a transition between BC and SBC regimes at a higher signal level. **Right:** a similar map; this time the agreement is shown as a function of the electron density distribution spread factors for the SBC regimes in the first and in the second CCD halves. This map shows that it is not possible to obtain a good agreement for a narrow electron density distribution in both CCD halves in the SBC regime (bottom left corner of the map).

measurement carried out by Astrium on an irradiated Gaia CCD and using a more sophisticated optimization procedure of the simulation parameters (see Fig. 6.10 right and Chapter 2). This deviation is thus more likely due to the limitations of the model itself than inherent to the rough optimization procedure used for the purpose of this chapter. However at lower signal levels ($< 10\,000$ e$^-$), the experimental data is reproduced within the noise by the simulation. Note that at very low signal levels (i.e. for a CI level < 100 e$^-$), the fractional charge loss measurement can be greater than 1. This would mean that the charge loss is greater than the number of charges originally available for trapping. This can of course not be simulated, and it is at present impossible to know why the data include such values.
Figure 6.11 (left and right) shows how the agreement between model and data varies as a function of some of the free parameters of the simulation. This agreement is quantified by a normalized χ^2 that is the χ^2 as defined in Section 6.4.3.3 normalized by the best agreement obtained as a result of our optimization procedure. The free parameters of interest are the electron density distribution spread factors for the SBC regime in the first half of the CCD η_1 and the second half η_2, as well as the signal at which the transition between SBC and BC regimes occurs S_{SBC_1} in the first half of the CCD. The presented maps allows us to characterize the values that these parameters must take for a reasonable agreement to be achieved.
Figure 6.11 (left) shows that a good agreement cannot be obtained in general for low values of the spread factor ($\eta_1 < 0.2$) i.e. for a narrow electron distribution when the electron packet sits in the SBC of the CCD upper half. The best fit occurs at $\eta_1 \approx 0.65$, which gives $\sigma_{y,\text{SBC},1} \approx 1.3$ μm and $\sigma_{z,\text{SBC},1} \approx 0.065$ μm. Fig 6.11 (left) also shows that if the transition between SBC and BC regimes occurs at relatively high signal levels (> 2000 e$^-$) in the CCD upper half, the electron distribution must be wide in this same half ($\eta_1 > 0.8$). Fig. 6.11 (right) shows that as expected a good agreement cannot be obtained for a narrow electron density distribution in both CCD halves for the SBC regime. It also shows that as long as the distribution of the electron density is wide in the CCD upper half a good agreement can be obtained independently of the distribution spread factor in the lower half.

6.4.5 Discussion of FPR measurements

The best fit to data from all stitch blocks with suspected working SBCs in the CCD upper half (right side of Fig. 6.10) finds $\sigma_{y,\text{SBC},1} \approx 0.2$ μm. However, the best fit to data (left side of Fig. 6.10) from one stitch block AL couple (see Fig. 6.5) with suspected non-functional SBCs in the stitch block in the CCD upper half finds $\eta_1 = 0.65$ (Fig. 6.11 left), where $y_{\text{SBC,max}} = 2$ μm so $\sigma_{y,\text{SBC},1} = 1.3$ μm. The right side of Fig. 6.11 gives $\eta_2 = 0.089$ in the lower half stitch block so $\sigma_{y,\text{SBC},2} \approx 0.2$ μm. Given that the nominal doping widths are 3 and 4 μm in the upper and lower halves of the Gaia CCDs, it is unphysical that $\sigma_{y,\text{SBC},1}$ is nearly 7 times larger than $\sigma_{y,\text{SBC},2}$. We interpret this evidence as being due to non-functional or missing SBCs in the upper half stitch block but SBCs present in the lower half stitch block. If there are no SBCs or very small SBCs in the upper half stitch block, our model fit tries to find a no-SBC regime as soon as possible, which corresponds to the electron distribution being as large as possible (i.e. emulating the BC distribution). This is what our model is doing with this stitch block AL couple data,

supporting our hypothesis that the SBCs are absent in the upper half of this particular stitch block AL couple.
The alignment of the photo-lithographic masks to make each stitch block partly depends on the alignment of the previous stitch block in the AC direction. It is possible that the random alignment errors introduced in each stitch block affect the next stitch block in the AC direction so that stitch errors compound, reaching their maximum furthest from the readout node, i.e. the stitch error diverges as a function of AC like a zip coming undone. Gaia CCDs contain nine stitch blocks and eight inter-stitch block aligments in the AC direction so the worst-case stitch error could be $8 \times 0.25 = 2$ μm. Seabroke et al. (2010) Fig. 5 shows that an AC displacement of 2 μm in SBC doping is enough for SBCs to be absent from upper half stitch blocks and to explain SBC FWCs of a few thousand electrons in lower half stitch blocks. e2v consider it improbable that these tolerances would all add cumulatively and the square root of the sum of the squares assumption for uncorrelated error sources (0.7 μm) is believed to be more representative. This means that the worst-case stitch error can only occur in the stitch block furthest from where the stitching begins, which is at the readout node end.
The bottom plot of Fig. 6.9 shows the data from three candidate stitch block AL couples with suspected absent SBCs in the stitch block in the upper half of the CCD. Fig. 6.5 shows that the strongest and one other candidate are indeed the termination stitch block AL couples furthest from the readout node. The data of the other termination stitch block candidate does not extend to small enough signal levels to distinguish whether the trend will turn over, indicative of the presence of working SBCs, or continue to rise like the strongest missing SBCs candidate. The other candidate is the seventh stitch block AL couple from the readout node and so its worst-case stitch error could be $6 \times 0.25 = 1.5$ μm. Seabroke et al. (2010) Fig. 5 shows that this is enough for SBCs to be absent from the upper half stitch block. However, its trend may be turning over, indicative of the presence of working SBCs.

6.5 Pocket pumping measurements

Fig. 6.12 (left) shows that each e2v Gaia silicon wafer can only include two Gaia CCDs (CCD91-72). The room left on each wafer was used for test structures that were included to assess the radiation hardness of Gaia CCDs. In order for these test structures to be irradiated and tested, they have to be packaged. e2v packaged up two CCD221 test structures for the e2v centre for electronic imaging at The Open University to test (see Fig. 6.12 right). Because they have the same pixel architecture (and thus manufacturing processes) as Gaia CCDs, we have repeated the pocket pumping measurements conducted by Kohley et al. (2009) to test whether these test structures also have missing SBCs. Kohley et al. (2009) tested an AF FM CCD with serial number 05486-11-02. The test structures are also post-2004 but from two different batches: 06026-16-04 and 06095-09-04 [2]. The last two digits are the position of the CCD on the wafer: 03 and 04 are the two side positions for the CCD221 test structures.
All CCD221 test structures have 1440 TDI lines and 224 columns, which is smaller than

2. 06095-09-04 is still to be tested and its results will be included in the submitted version of this chapter.

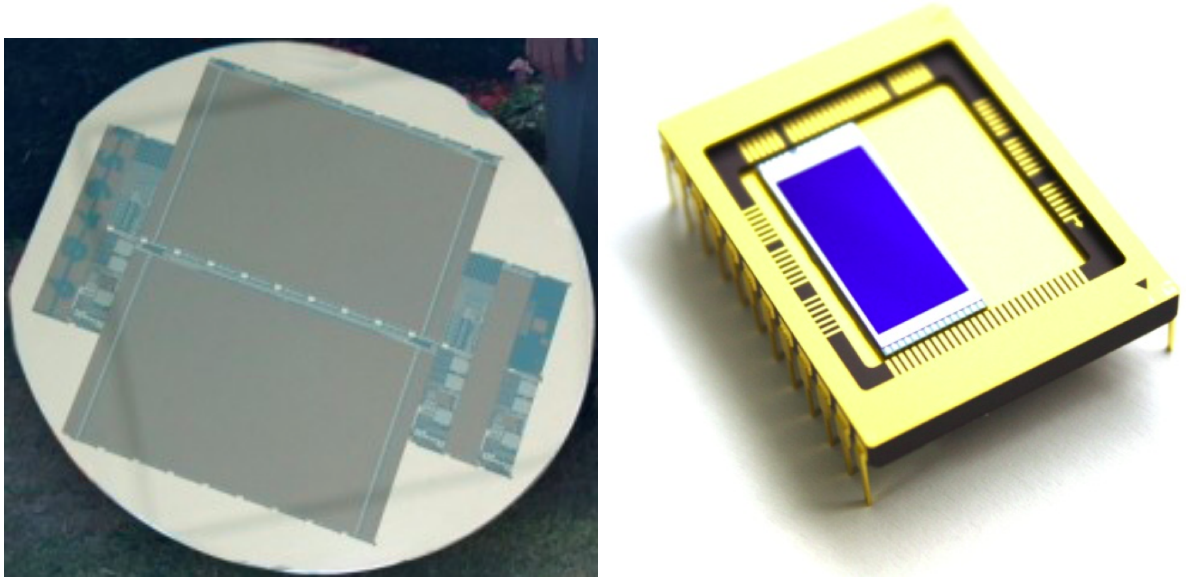

Figure 6.12 — Left: e2v Gaia silicon wafer with photoactive regions (dark grey) showing two CCD91-72s in the centre and small test structures on either side. The photoactive strip on the right side is two CCD221s abutted. **Right:** Gaia test structure CCD221 packaged for use. (Images courtesy of e2v technologies.)

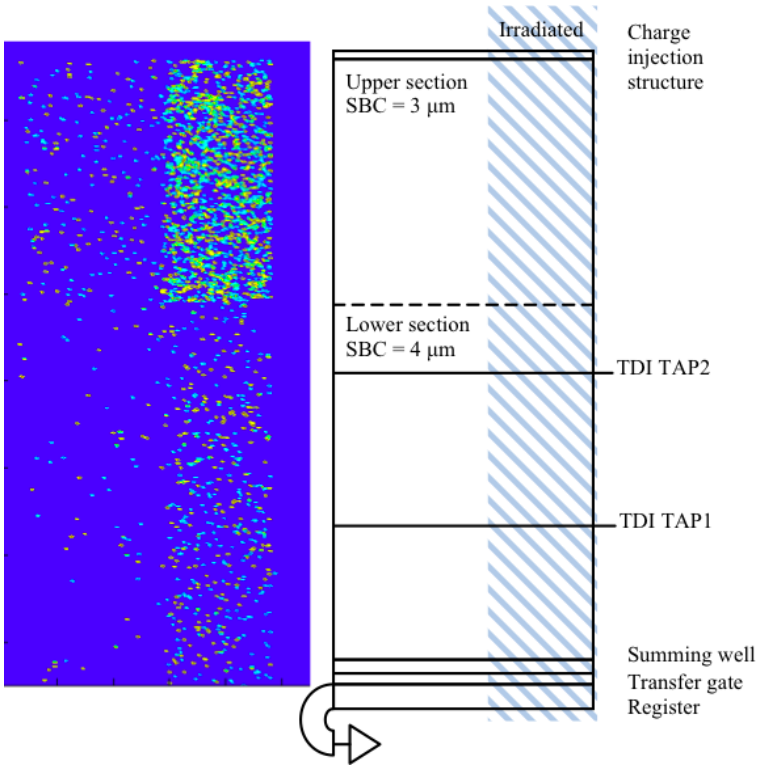

Figure 6.13 — Left: Image of a pocket pumping measurement of test structure CCD221 (serial number 06026-16-04) showing forward (yellow dots) and reverse (cyan dots) traps. **Right:** Layout of all CCD221 test structures and the area of 06026-16-04 that was subjected to proton irradiation to a 10 MeV equivalent dose of 1×10^9 protons cm^{-2}.

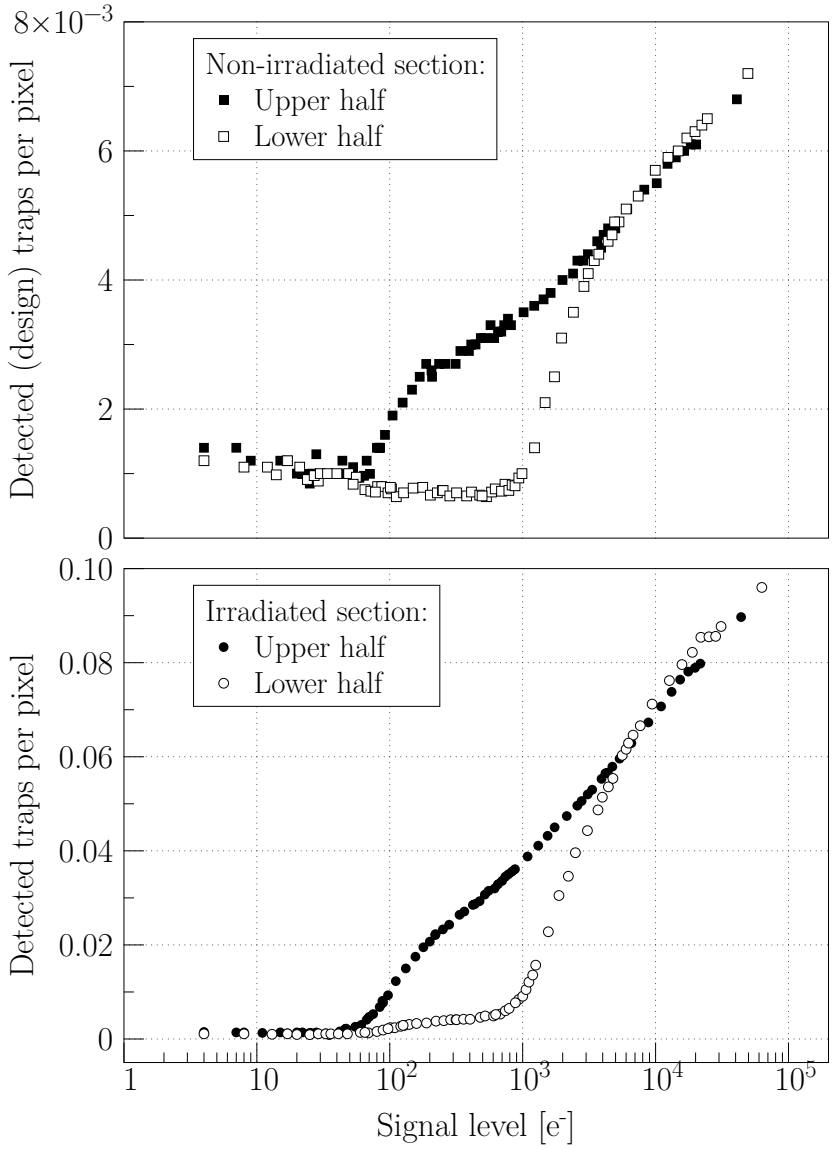

Figure 6.14 — Number of detected traps per pixel as a function of signal level. **Top:** Fabrication or design traps (see left side of pocket pumping image and left side of layout schematic in Fig. 6.13). **Bottom:** Radiation traps (see right side of pocket pumping image and right side of layout schematic in Fig. 6.13).

one Gaia stitch block (2160 or 2340 TDI lines and 250 or 108 columns). The dotted line in Fig. 6.13 is the only stitch boundary in the CCD221 test structure, showing it consists of two stitch blocks: two AL stitch blocks in one AC position (i.e. the CCD221 test structure cannot be used to compare stitch blocks in different AC positions as was done in Kohley et al. 2009).

Fig. 6.14 shows that the number of identified fabrication traps per pixel in CCD221 test structure 06026-16-04 is the same order of magnitude as seen in AF FM CCD 05486-11-02 (cf. Kohley et al. 2009 Fig. 9). It also shows that there are an order of magnitude more radiation traps per pixel as there are fabrication traps per pixel but that both types of trap follow the same trends as a function of signal size, depending on whether

they are in the upper or lower half of the test structure. These trends as a function of signal size are that in the lower half, signals < 1000 e$^-$ have a very different gradient to signals > 1000 e$^-$. We interpret the change in gradient as due to electrons spilling out of SBCs with FWCs of ≈ 1000 e$^-$. This is consistent with the spread of SBC FWCs found by Kohley et al. (2009). Like their Fig. 9, the upper half does not exhibit a change in gradient at ≈ 1000 e$^-$. We interpret this as strong evidence for no working SBCs in the upper half of this device. The number of traps in both halves of the device and both trap types converge at ≈ 65 e$^-$. Charge packets may need volumes greater than the volume of a charge packet containing ≈ 65 e$^-$ in order to be captured by more than the minimum trap density in this device. However, Kohley et al. (2009) Fig. 9 shows that their device has not reached its minimum trap density at 40 e$^-$.

6.6 Comparison of Radiation Campaigns 3 and 4 test data from the same CCDs

Both experimental and theoretical studies show that CTI drastically decreases the quality of stellar images as collected by the Gaia CCDs. On top of a significant charge loss, CTI induces an image distortion that introduces a systematic bias in the image location estimation. This affects the Gaia image location accuracy and consequently the final astrometric accuracy. It is for this reason that Astrium have carried out a series of 4 test campaigns on a small number of irradiated CCDs in order to evaluate the impact of radiation damage on the image parameter estimation and ultimately on the Gaia astrometric performances. Table 6.3 provides a summary of the CCDs tested during these campaigns. Each experimental test was carried out in order to study a range of differing effects (i.e., to examine the influence of a diffuse optical background on the CTI, to optimise CI parameters, to examine the CTI in the serial register, to address the reduction in CTI due to the recent transit of other stars etc.) and here we present a subset of the results from the analysis of these data. Note that a fifth campaign RC5 is currently in preparation.

The location biases of the images are generally calculated through an analysis of data obtained from a number of runs of an illuminated mask along the CCD which is operated in TDI mode. A number of different masks were used throughout the testing campaigns, each with a different pattern of pin-holes (of sometimes differing diameters). The goal is to simulate the accumulation of stellar images on the CCD as the mask is translated in synchronous timing with the clocking speed of the detector. The general procedure for deriving the location bias values due to radiation-induced CTI is as follows. Stellar images are accumulated from a portion of the CCD that has no radiation damage and the measured locations are then compared to the measured image locations derived from those data which originate from the irradiated region. A number of 'stars' on the mask are always detected in a damage-free region which permits the mask-displacements and illumination variations to be calibrated out. The charge loss measurements are calculated in a similar manner. An exception to this method of location bias determination occurs for a subset of data from RC3 and RC4 which was acquired using a 'sky-like' mask with a pseudo-realistic sky-pattern. This mask is passed along the detector at a number of differing AC locations and, crucially, these runs also were repeated with the mask rotated 180° with respect to the CCD. This al-

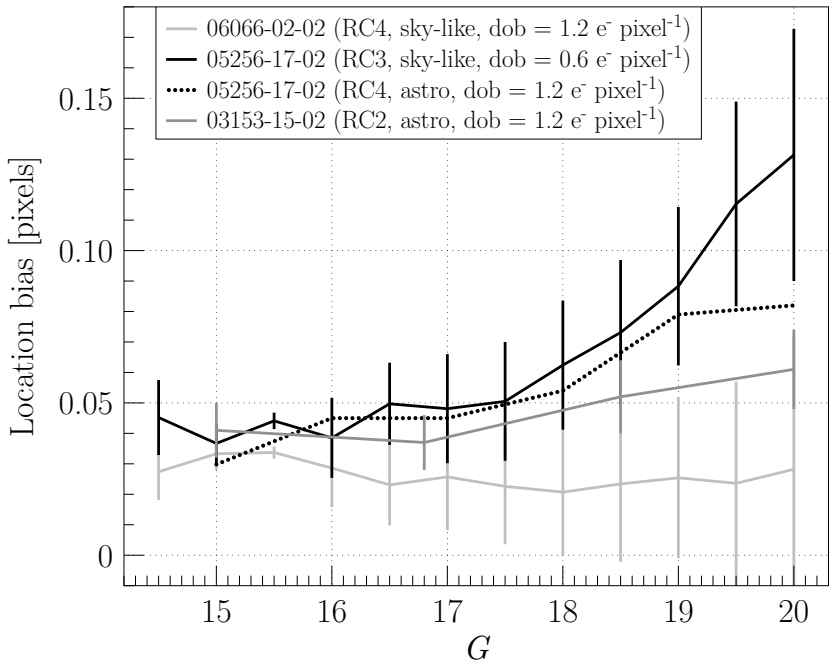

Figure 6.15 — Stellar image location bias values calculated through the analysis of data from a partially irradiated CCD using a mask with pseudo sky-patterns of pin-holes and CI interval of 1 s. A fully-functioning SBC should mitigate the location bias for faint stars, however a clear difference between the bias values obtained from the 05256-17-02 CCD (black line) and the two other CCDs used in campaigns 2 and 4 is apparent. This strongly suggests that SBCs in the 05256-17-02 CCD are not fully effective. See text for further details.

lows the location bias to be separated from calibration effects and for the bias values and calibration parameters to be solved for using a least-squares solution.

The resulting bias measurements shown in Fig. 6.15 differ between RC2, RC3 and RC4 at faint magnitudes: the RC3 data does not plateau to an approximately constant bias at faint magnitudes. This is in contrast to the data from the other campaigns. One possible reason for the RC3 bias values not plateauing is due to the presence of the constant diffuse optical background (DOB) being better controlled in the experimental set-up of RC3 compared to RC2 and RC4. When the DOB is very close to zero, then just a small amount of background light can vastly reduce image location bias due the resulting photoelectrons keeping many of the traps with long time constants (or 'slow' traps) filled. Indeed, the measured DOB levels are ~ 0.5 e$^-$ pixel^{-1} at readout lower in the RC3 data than in the RC4 data. However, data taken with the same CCD as was used in RC3 shows a similar bias function (i.e., no plateau at faint magnitudes) and in this case the DOB level is comparable to both the RC2 and RC4 data set. It thus appears that the DOB level is not the primary cause of the discrepancies between the location bias functions across the different test campaigns. This hypothesis is further strengthened when one considers that these data were obtained using a CI every second, which also has the effect of keeping the 'slow' traps filled, and making the effect of small levels of DOB much less significant. The most likely conclusion is that the measured differences are intrinsic to the CCDs and likely due to a lower functional ef-

ficiency of the SBCs in the upper half stitch blocks where the test data was taken from 05256-17-02.
Table 6.3 also summarises which of the RC CCDs are affected by the SBC issue. Fig. 6.15 shows that 03153-15-02's location bias as a function of brightness is in between the plateau of 06066-02-02 (likely functional SBCs) and 05256-17-02 (likely non-functional SBCs). However, the discussion in Section 6.3.1 of Fig. 6.10 (right) has already established that 03153-15-02 is not affected by the SBC issue. The RC data obtained from 06244-03-01 and 06273-08-01 was not designed to test SBC efficiency but it could potentially be modelled by CEMGA to determine whether these CCDs are affected by the SBC issue.

6.7 Discussion

6.7.1 Non-functional SBC statistics and predictions

e2v changed their photo-lithographic mask set in 2004. The mask set used to manufacture pre-2004 CCDs was meant to be identical to the mask set used to manufacture post-2004 CCDs. In order to test this assertion we consider evidence from the pre-2004 and post-2004 CCDs separately. Because of the low number of CCDs that have been tested, we augment our evidence found in this chapter with evidence from the literature.

Pre-2004 CCDs:
From the Sira test sample, out of the seven 2003 AF CCDs searched for evidence of missing SBCs in Section 6.4, we only find one CCD with one stitch block AL couple (termination stitch block with 108 columns) strongly suspected of not having SBCs in the upper half stitch block. We augment this pre-2004 CCD sample with the first device tested by Astrium, an AF DM (03153-15-02) that exhibits operational SBCs in all its AL stitch block couples (see Fig. 6.10). Thus, the SBC issue in the pre-2004 CCD sample of Gaia CCDs affects:
– 1 out 8 CCDs $= 12.5\%$ of CCDs;
– 1 out of $(9 \times 8 =)$ 72 stitch block AL couples in 8 CCDs $\sim 1.4\%$ of stitch block AL couples;
– 108 out of $[9 \times (2 \times 108 + 7 \times 250) =]$ $15\,728$ columns in 8 CCDs $\sim 0.7\%$ of columns.
This small number of columns with missing SBCs in their upper halves is consistent with accumulating stitch errors at each of the eight inter-stitch block AC alignments being a rare event, mainly in the termination stitch blocks furthest from the readout node.

Post-2004 CCDs:
In Section 6.5, we found one CCD221 test structure without SBCs in its upper stitch block (224 columns). In Section 6.6, two post-2004 devices have been tested by Astrium out of which one shows evidence for a non-functional SBC in its upper half (2 stitch block AL couples tested) and one appears not to be affected (5 stitch block AL couples tested). To this one case we add the device tested by Kohley et al. (2009) (9 stitch block AL couples affected). This means the SBC issue in the post-2004 sample of Gaia CCDs affects:
– 3 out 4 CCDs $= 75\%$ of CCDs;

– $(1 + 2 + 9 =)$ 12 out of $(1 + 2 + 5 + 9)$ 17 stitch block AL couples tested in 4 CCDs ∼71% of stitch block AL couples;
– $(224 + 500 + 1966 =)$ 2690 out of $(224 + 500 + 1250 + 1966 =)$ 3940 columns tested in 4 CCDs ∼68% of columns.

The difference between the number of columns with missing SBCs in their upper half in the pre- and post-2004 CCD samples was evaluated statistically using the χ^2 test. The difference between the two samples was shown to be highly statistically significant ($\chi^2 \sim 1{\times}10^4$, $p < 5{\times}10^{-8}$). Therefore the null hypothesis that the number of columns with missing SBCs in their upper half is the same in both the pre- and post-2004 CCD samples is rejected at the $>5\sigma$ significance level. This points to a change in e2v manufacturing of Gaia CCDs between 2003 and 2005. There are no post-2004 CCDs with some upper half stitch blocks affected by the SBC issue and others not. This suggests that a rare compounding of stitch errors is not responsible but a more systematic change in manufacturing has occurred since 2003. The different mask set is the only known change between 2003 and 2005. The two mask sets were meant to be identical but a large mask writing error may have occurred in the manufacture of the post-2004 mask set.

Gaia CCDs were front-face processed first and then back-face processed. Front-faced processing is when the electrodes are made and all doping implanted and is batch based. Because all the Gaia CCDs have the same pixel architecture, front-face processing is the same for all Gaia CCDs: AF, Blue Photometer (BP), Red Photometer (RP). e2v and Astrium refer only to these CCD variants as the Radial Velocity Spectrometer (RVS) CCDs are identical to RP CCDs. Table 6.4 shows that back-face processing is different for the different types of Gaia CCD and is wafer-based. Each CCD serial number encodes when the front-face processing occurred but not when the back-face processing occurred, which can be much later.

The fact that the SBC issue is only related to front-face processing and all the wafers in a batch have the same nominal front-face processing means that if a CCD of any type is found to be affected by the SBC issue, then all the CCD variants (AF, BP and RP) from that batch are likely to also be missing SBCs in their upper half stitch blocks. Table 6.5 summarizes the CCDs already tested for SBC efficiency and those that could be tested in the future. They are all from different batches so whether other CCDs from the same batch are also affected remains unproven (none of the DM or EM CCDs are from these three affected batches either). In the absence of evidence demonstrating that all CCDs from the same batch have the same SBC properties, we can only tentatively predict which FM CCDs are likely to be affected by the SBC issue, based on e2v's premise that all CCDs from the same batch are nominally the same (see Table 6.6), and which are currently assigned to Gaia's Focal Plane Array (FPA, see Fig. 6.16 and Table 6.7).

The four CCDs tested for the SBC issue in Table 6.5 are from four different batches, one of which does not include any FMs. Fig. 6.16 and Table 6.7 show that the remaining three batches that include FMs only include 19% of the CCDs that currently make up Gaia's FPA and for which tentative predictions of which are affected or not can be made. Fig. 6.17 shows the 106 CCDs that currently make up Gaia's FPA come from 32 different batches. Therefore, the 81% of CCDs that currently make up Gaia's FPA and for which tentative predictions cannot be made come from 29 completely untested

batches. Table 6.6 shows that some of the batches include flight spares. Like the FPA-assigned CCDs, the flight spare CCDs are also coupled to FM Proximity Electronics Module (PEM). The clock timing of PEMs does not allow modification for backwards shifts in the image area for pocket pumping. In case the currently FPA-assigned CCD and PEM couples need to be replaced, the flight spare CCD and PEM couples cannot be decoupled (and thus pocket pumped) until after Gaia is launched.
After launch, the CCDs on board can in principle be tested using CI MIM. If SBC FWC needs to be characterised before then, in principle all the test structures that were on the same wafers as the 106 Gaia CCDs that will actually fly could be tested using the pocket pumping technique. However, to obtain these may require paying e2v to package all these test structures to allow them to be tested. This would be the definitive method to resolve the SBC issue but could be very expensive and the testing could be very time consuming. A cheaper and quicker solution would be to establish how likely all the wafers in a single batch have the same SBC properties. This could be done by getting the test structures from the same batch but different wafer as the already tested CCDs in Table 6.5. If the test structure pocket pumping results agree with the results in Table 6.5 then e2v's premise that all CCDs from the same batch have the same SBCs will be supported by evidence and the tentative predictions of which FPA CCDs are likely to be affected by the SBC issue and which are not will be less tentative.
Table 6.7 shows that 17% of FPA CCDs are likely to be affected by the SBC issue. Given that only three out of the 32 FPA batches have been tested, 17% represents a likely minimum number of FPA CCDs affected. All the post-2004 evidence suggests that if a CCD is affected by the SBC issue, then all its upper half stitch blocks are affected. We can predict the fraction of CCDs that will be affected by continuing with the assumption that if a batch is affected by the SBC issue then all CCDs in that batch will be affected. We only have test data for four post-2004 batches, three of which were affected by the SBC issue. To predict the fraction of affected FM CCDs in the batches not examined so far and quantify the uncertainty on this number we use the following simple statistical model. We assume that there is a certain probability θ that a given batch suffers the SBC issue, and that the number of affected batches follows from a Bernouilli trial with probability θ. From the batches tested we know that θ is most likely 0.75, but the distribution of possible values of θ is rather wide because we only have a small number of tested batches. In this statistical model θ is given by a $B(4,2)$ distribution, with $B(x,y)$ the Beta function. From this distribution it follows that with 99% confidence $0.19 \leq \theta \leq 0.98$. We can now simulate a Bernouilli trial for the untested batches in order to predict the number of FM CCDs affected by the SBC issue. In the simulation we draw a random θ from the $B(4,2)$ distribution and then perform a Bernouilli trial for the 29 untested batches. In each trial we keep track of which batch from Fig. 17 was affected and add the corresponding number of CCDs to the total. In this way we can predict the distribution of the fraction of affected FM CCDs in the untested batches. Not surprisingly the median of the distribution is at 69%. However, the inter quartile range and the 99% range are 52–83% and 11–100% respectively, reflecting the small number of batches on which we base our extrapolation.

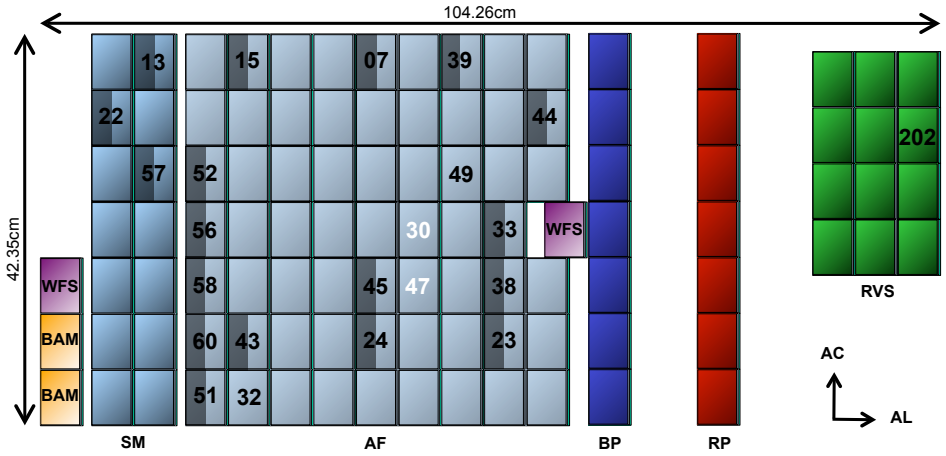

Figure 6.16 — Gaia's FPA shows the current assignment of FM CCDs (subject to on-ground testing or other Assembly, Integration, and Verification (AIV) procedures, CCDs can still be replaced by flight spares). The shaded regions indicate which CCDs from Table 6.6 are likely to be affected by the SBC issue with Astrium FM numbers in black. Numbers in black without shaded regions on AF CCDs indicate CCDs from a batch 06095-XX-0X which may or may not be affected by the SBC issue, depending on the pocket pumping results from test structure 06095-09-04, which will be included in the submitted version of this chapter. The number in black without a shaded region on one of the RVS CCDs indicates that this FM CCD is from the batch 06273-XX-0X, which includes 06273-08-01 (one of the RC CCDs, see Section 6.6). 06273-08-01 could either be pocket pumped in RC5 or previous RC data could be modelled to determine whether it, and so also the RVS FPA CCD from the same batch, are affected by the SBC issue. White numbers indicate CCDs currently integrated into the FPA are from the same batch (06066-XX-0X) as the FM CCD with likely working SBCs in its upper half (06066-02-02, see Section 6.6) are so are also likely to be fully functional. Background diagram courtesy of A. Short (ESA, ESTEC)

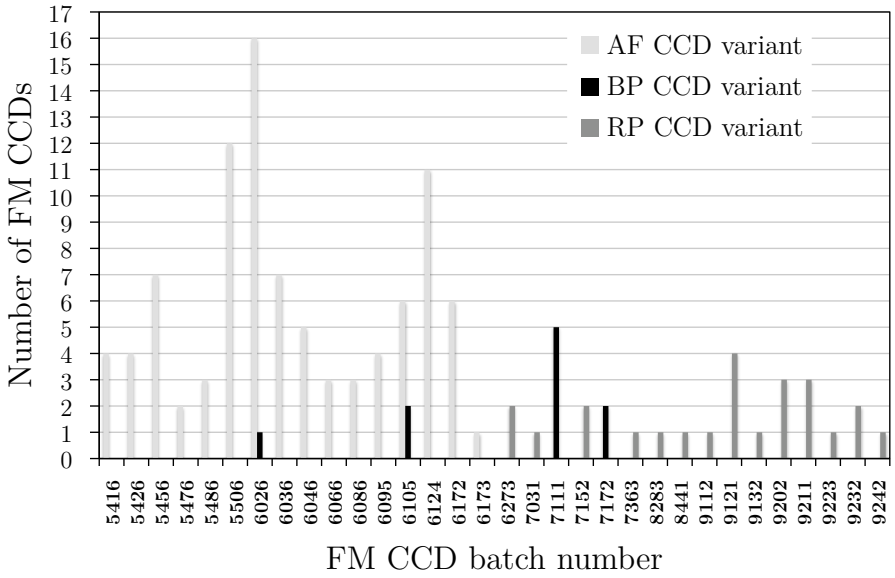

Figure 6.17 — Number of FM and spare CCDs (AF, BP and RP variants) chronologically plotted as a function of batch number.

Serial Number	Variant	Affected
03153-15-02	AF DM	N
05256-17-02	AF EM	Y
06066-02-02	AF EM	N
06244-03-01	RP DM	?
06273-08-01	RP EM	?

Table 6.3 — Summary of the CCDs tested during Astrium's RCs. Affected indicates whether the CCD is likely to be affected by the SBC issue (Y), likely to have fully functional SBCs (N) or yet to be tested for SBC efficiency (?).

CCD	d	Surface	λ	Instrument (number of CCDs)
AF	16	Basic	650	AF (62), SM (14), WFS (2)
BP	16	Enhanced UV	360	BP (7)
RP	40	Basic	750	BAM (2), RP (7), RVS (12)

Table 6.4 — Comparison of back-face processing between the Gaia CCDs. d is the depth the wafer was thinned to in μm. Surface passivation was annealing "dangling bonds" with hydrogen gas at high temperatures to reduce dark current. All the Gaia CCDs have a single layer Hafnium oxide anti-reflection coating but each variant has its coating centred on a different wavelength (λ in nm). The other Gaia instruments are Sky Mapper (SM), WaveFront Sensor (WFS) and Basic-Angle Monitoring (BAM).

Method	Variant	Serial Number	Batches	Affected
RC3&4 (this chapter: re-analysis)	AF EM CCD	05256-17-02	05256-XX-0X	Y
PP (Kohley et al. (2009): measurements & analysis)	AF FM CCD	05486-11-02	05486-XX-0X	Y
PP (this chapter: 1st measurement & analysis)	AF FM test structure	06026-16-04	06026-XX-0X	Y
RC4 (this chapter: re-analysis)	AF EM CCD	06066-02-02	06066-XX-0X	N
PP (undergoing: 1st measurement & analysis)	AF FM test structure	06095-09-04	06095-XX-0X	?
RC5 PP? (recommendation of this chapter)	RP DM CCD	06244-03-01	06244-XX-0X	?
RC5 PP? (recommendation of this chapter)	RP EM CCD	06273-08-01	06273-XX-0X	?

Table 6.5 — Measurement method used to test FM CCDs and test structures, where PP is pocket pumping and RC is analysis of Radiation Campaign data, e2v serial numbers of the tested devices and the FM batches likely to be affected by the SBC issue (Y), likely to have fully functional SBCs (N) or yet to be tested for SBC efficiency (?). Only FM CCDs will be flown on Gaia and all FM CCDs were built post-2004 so this table excludes 03153-15-02 (RC CCD shown not be affected by the SBC issue) and 03153-20-01 (the one pre-2004 CCD found with missing SBCs in one of its upper half stitch blocks).

6.7.2 Impact on the Gaia image location accuracy

Gaia has been designed to perform absolute astrometric measurements at very high accuracy. As the estimated image location for all CCD observations are ultimately used to derive the star astrometric parameters, the requirements on the image quality are very stringent. CTI distorts the image and decreases the signal-to-noise ratio. While the image distortion, if not properly taken into account, introduces a significant bias (e.g., Fig. 6.15) in the image location estimation, the decrease in signal-to-noise ratio implies an irreversible loss of accuracy independent of any estimator. Chapter 3 presents an accurate and detailed evaluation of the two effects. Their results were obtained by simulating numerous damaged and CTI-free stellar transits for different CCD operating conditions but assuming properly working SBCs; they used parameters for the electron density distribution derived from the FPR measurement based on the CCD 03153-15-02 with functional SBCs. We are now interested in repeating the same experiment with parameters for the electron density distribution in the SBC regime derived from the FPR measurement based on the CCD 03153-20-01 with non-functional SBCs in the upper CCD half (see Section 6.4.4).

Figure 6.18 (top) shows the relative loss of accuracy in image location as a function stellar magnitude. This is computed by comparing the theoretical limits (the Cramér-Rao bounds) to the image location accuracy for a damaged and a CTI-free Gaia-like image. Zero loss of accuracy corresponds to the CTI-free case (for more details see Chapter 3). Fig. 6.18 (bottom) shows the image location bias as a function stellar magnitude. It is obtained by applying the Gaia image location procedure to several hundreds of profiles without applying any CTI mitigation procedures, the bias itself is computed by subtracting the true from the estimated location. Fig 6.18 provide a comparison for three different cases: (i) the Gaia nominal case i.e. functional SBCs in both CCD halves (blue continuous line), (ii) non-functional SBCs in the CCD upper half (red dashed line), and (iii) no SBCs at all (black dotted line). The middle case corresponds to the most realistic case for Gaia CCDs containing non-functional SBCs as identified in this chapter. For the simulation we used an active trap density of 1 trap pixel^{-1}. This particular density was shown in Chapter 3 to reproduce the amplitude of location bias measured using experimental test data taken 1 s after a CI and for a Gaia irradiated CCD with a radiation dose of 4×10^9 protons cm^{-2} (10 MeV equivalent). This dose corresponds to the upper limit of the predicted accumulated radiation dose for the Gaia nominal lifetime.

From both figures it is clear that a non-functional SBC in the CCD upper half degrades the location precision and introduces a greater bias for the faint magnitudes ($G > 15$), however it is not as severe as for the no SBC (in both halves) case. At magnitude 20 both precision and bias are worse by a factor 2. A 10% decrease in image location accuracy is acceptable and does not threaten the Gaia requirements. The bias can in principle be calibrated out by using the same mitigation procedure as foreseen in the case of nominal CCD functioning. The modelling used in the mitigation procedure will however have to be modified so that a missing SBC in a fraction of the AL stitch block couples can be accounted for.

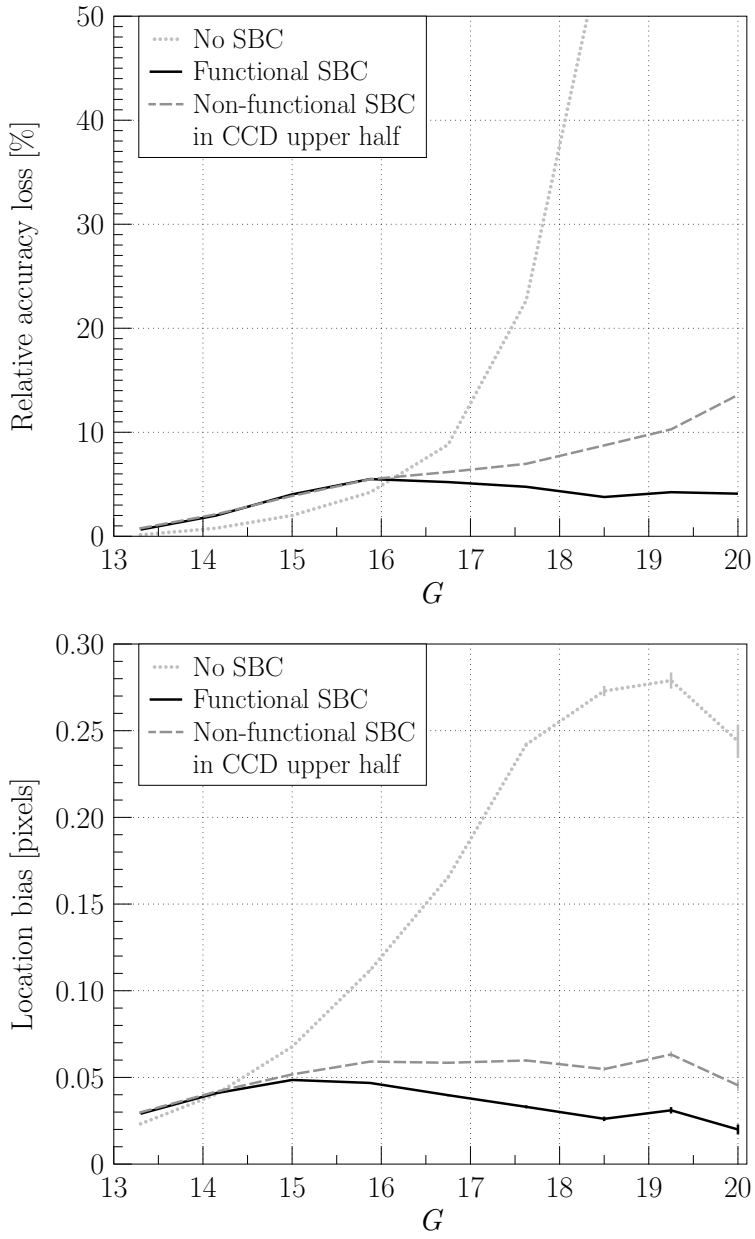

Figure 6.18 — Predicted end-of-life relative image location accuracy loss (top) and bias (bottom) as a function of magnitude (G-band) for a 1 s CI delay and three different pixel architecture cases: (i) functional SBCs in both CCD halves (blue continuous line), (ii) non-functional SBCs in the CCD upper half (red dashed line), and (iii) no SBCs at all in both CCD halves (black dotted line). **Top:** The non-functional SBC cases (ii) and (iii) only affects the faint signals ($G > 15$). For case (iii) the loss of accuracy is dramatic: 200% for $G = 20$ (not shown for readability), however, as explained, in the text this is not what is expected for Gaia. For cases (i) and (ii), representative of the Gaia CCD with respectively functional and non-functional SBCs the CTI-induced loss of accuracy does not exceed 10%, which is acceptable regarding the Gaia requirements (Chapter 3). **Bottom:** The CTI mitigation procedure enables a 90% recovery of the bias (Chapter 3), bringing back the residual bias to an acceptable level for cases (ii) and (iii). Error bars represent the statistical uncertainty, not the standard deviation. Note that here no mitigation procedure at the image processing level was applied.

6.8 Conclusions

We have re-analysed the Hopkinson (2006) data set of First Pixel Response (FPR) measurements of seven Gaia Engineering Model (EM) CCDs. This data is grouped according to how e2v manufactured the CCDs: stitch blocks, which correspond to the size of the photo-lithographic mask used to implant doping features that define the pixel architecture. Because Gaia operates in Time-Delayed Integration (TDI) mode, observations are transferred through two stitch blocks in the ALong scan (AL) direction before being read out. The FPR data therefore samples these stitch block AL couples. We only find one stitch block AL couple (the termination stitch block AL couple at the end of the CCD, consisting of 108 columns) in one of these CCDs where the FPR curve does not exhibit the characteristic bump of the supplementary buried channel (SBC, otherwise known as a notch or mini-channel).

Modelling this termination stitch block AL couple with a detailed electrode-level model finds a best fit where the electron distribution within the SBC is not confined to a narrow region as expected in the upper half of the CCD but is confined in the lower half. Its distribution in the upper half is more like a buried channel (BC), whereas it is like a SBC in the lower half. This suggests the stitch block in the upper half of the CCD does not have SBCs. The reason for missing SBCs and measured SBC Full Well Capacities has been explained by the SBC doping abutting the anti-blooming drain (ABD) and the ABD shielding doping cancelling out much of the SBC doping, reducing the SBC potential to much smaller than designed (Seabroke et al. 2010).

Evidence for missing or non-functional SBCs in the upper half has already been published (Kohley et al. 2009) but this was found in only one CCD. Based on our modelling results and the effects of CTI on artificial stellar images we can infer the presence of non-functional SBCs in the upper half of the CCDs tested by Astrium during their Radiation Campaigns (RCs). To the seven Astrometric Field (AF) CCDs tested by Hopkinson (2006), we add the results of one test structure tested by us and four more AF CCDs tested by Astrium and the results of Kohley et al. (2009) and thus present the largest sample of Gaia CCDs to be analysed for the presence of SBCs. The difference between the number of columns with missing SBCs in their upper half in the pre- and post-2004 CCD samples is highly statistically significant ($>5\sigma$), pointing to a change in e2v manufacturing of Gaia CCDs between 2003 and 2005. Different photo-lithographic mask sets is the only known change between 2003 and 2005.

The fact that the SBC issue is only related to front-face processing and all the wafers in a batch have the same nominal front-face processing means that if a CCD of any type is found to be affected by the SBC issue, then all the CCD variants, AF, Blue Photometer (BP) and Red Photometer (RP), from that batch are likely to also be missing SBCs in their upper half stitch blocks. By comparing the batch numbers of the three affected FM CCDs (three different batches) with those currently assigned to Gaia's Focal Plane Array (FPA), we tentatively predict that a minimum of 17% of FPA CCDs (three Sky Mappers and 15 AFs) are likely to be affected by the SBC issue. In the absence of further testing, we predict that in the other 29 completely untested batches 69% of the CCDs may be affected (between 11 and 100% with a 99% confidence interval). Therefore, despite different CCD manufacturers, it appears likely that the majority of Gaia's

106 CCDs have the same missing SBC issue as the two CCDs in Hubble's Advanced Camera for Surveys (ACS)/Wide Field Channel (WFC), albeit only in the upper half of Gaia's detectors.

By analyzing the data from Astrium RCs, this chapter has also addressed whether SBCs were working properly in Gaia CCDs used to predict the mission performances and against which CTI mitigation models are being developed and tested. We find that the AF CCD tested in RC3 appears to have non-functional SBCs in the upper half of the CCD region where the test data was obtained. The two other tested AF CCDs are not affected by this issue. This means that test data exists for predicting mission performances for CCDs with and without functioning SBCs in their upper halves and testing mitigation models. The limited test data available means we have only been able to demonstrate that non-operational SBCs are likely in AF FM CCDs. We show that for an AF CCD with non-operational SBCs in its upper half, the Gaia image location accuracy is affected by less than 10% if the CTI effects can be properly calibrated, which is within Gaia AF requirements. Future testing may reveal that other affected batches contain FM BP and RP variant CCDs. How this affects BP, RP and RVS science is beyond the scope of this chapter but should be investigated in case BP, RP or RVS Gaia science requirements are not met.

Gaia's CCDs have already been integrated into the Focal Plane Array by Astrium so it is too late to change which FM CCDs are selected to fly on Gaia.

If the SBCs need to be characterised before launch, then the likelihood of all the wafers in a single batch having the same SBC properties needs to be established. This could be done by getting the test structures from the same batch but different wafer as the already tested CCDs. If the test structure pocket pumping results agree with the extant results then e2v's premise that all CCDs from the same batch have the same SBCs will be supported by evidence and the tentative predictions of which FPA CCDs are likely to be affected by the SBC issue and which are not will be less tentative. If this is not possible, two of the three methods we have presented to measure the SBCs can be used in-flight: FPR and the minimum injection method (MIM). Pocket pumping cannot be used in flight because the clock timing in the Proximity Electronics Module does not allow modification for backwards shifts in the image area. In-flight tests only need to be conducted once for each CCD so it should be possible to schedule it before routine operations begin. FPR will be used anyway because it can measure radiation trap properties. However, it has the disadvantage of being model-dependent. MIM is a fast method that directly measures whether SBCs are present (see Recommendations in Section 6.9). The identification of CCD columns with non-operational SBCs will help the calibration of the CTI in all Gaia instruments and guarantee that at least the final astrometric accuracy of Gaia is preserved (the final photometric and spectroscopic accuracy still needs to be investigated).

It should be emphasized that SBC Full Well Capacity (FWC) has never been a formally agreed CCD acceptance criterion in the Gaia contract between ESA/EADS Astrium and e2v. For this reason, it was not tested very thoroughly in the Gaia development phase. A more detailed test plan that went beyond the CCD acceptance criteria would have found the SBC issue, maybe early enough to change the pixel design. The SBC issue is related to manufacturing alignment accuracy. We would recommend e2v to ei-

ther widen future SBCs if they are adjacent to ABDs to compensate for the SBC issue or place the SBC in the middle of the BC to avoid the issue completely but the technique used to manufacture Gaia's CCDs is a decade old and has been superseded by Nikon, which delivers five times better accuracy. The Nikon technique has not been used yet to manufacture SBCs, because the CCD industry now views SBCs as counter-productive. Nevertheless we demonstrate that the improvement in signal-to-noise ratio at low signal levels provided by functional or even partly-functional SBCs is critical to achieving the Gaia requirements; it is thus important that the industry pursues the development of such features to prepare for future space missions with stringent image quality requirement at low signal levels.

6.9 Recommendations

This paper can only tentatively predict how many CCDs on the Gaia satellite will be affected by the Supplementary Buried Channel (SBC) issue because the prediction uses e2v's assumption that all CCD batches will have nominally the same SBC characteristics. Therefore, the top priority is to directly measure Gaia CCDs for the SBC issue on the satellite prior to launch if possible. The quickest method to do this is the Minimum charge Injection Method (MIM). However, the efficiency of the method has not been demonstrated. In this context, we recommend the following:

1. Our highest priority recommendation is to test the efficiency of MIM. If our test structure that has not been pocket pumped yet is found to have working SBCs in its upper half, then we (NJM and AH) can test the efficiency of MIM with it. If the test structure is found not to have working SBCs in its upper half, then MIM should be tested on one of the CCDs shown in this paper to have working SBCs in their upper halves (pre- or post-2004 CCDs). It appears as though these tests will not be conducted by Astrium but we are investigating whether these CCDs can be loaned out from Astrium to allow these tests to take place.
2. If MIM efficiency is demonstrated, MIM should be included in on-ground testing or other Assembly, Integration, and Verification (AIV) procedures prior to launch.
3. If MIM efficiency is demonstrated but MIM tests cannot be performed prior to launch, they should be conducted post-launch during initial in-orbit calibration before nominal operations begin.
4. If MIM efficiency is not demonstrated and modelling mission data does not identify which CCDs are affected by the SBC issue but this information is required to mitigate the resulting increased radiation damage, then we recommend that First Pixel Response testing and modelling, as done in this paper, is included in-flight. When the CCDs are sufficiently irradiated, this could be scheduled during orbital maintenance manoeuvres during which nominal data acquisition is suspended for two hours once per month.

Acknowledgements

Dr. Gordon Hopkinson (1952-2010) of Surrey Satellite Technology Ltd., Sevenoaks, UK, kindly provided the data used in this chapter and was very supportive of the

project but sadly did not live to see it come to fruition. This chapter is dedicated to his enormous contribution to developing astronomical instrumentation in general and to measuring Gaia radiation effects in particular. We thank David Burt (e2v technologies plc, Chelmsford, UK) for Figures 6.1, 6.2, 6.3 and 6.4 and for his invaluable insight into the design and manufacturing processes of e2v's Gaia CCDs through his regular visits to the e2v centre for electronic imaging at The Open University, UK. GMS is funded by the UK VEGA Gaia Data Flow System grant. The work of TP was supported by the European Marie-Curie research training network ELSA (MRTN-CT-2006-033481).

Batch	FM	Serial number	Affected
05256-XX-0X	None	None	Y
05486-XX-0X	FM07	05486-04-02	Y
	FM06*	05486-12-02	Y
	FM13	05486-15-02	Y
06026-XX-0X	FM52	06026-02-02	Y
	FM15	06026-06-01	Y
	FM44	06026-07-02	Y
	FM51	06026-09-02	Y
	FM33	06026-11-01	Y
	BPFM101*	06026-12-02	Y
	FM38	06026-13-01	Y
	FM39	06026-14-01	Y
	FM22	06026-15-02	Y
	FM58	06026-17-02	Y
	FM43	06026-18-01	Y
	FM45	06026-18-02	Y
	FM57	06026-19-02	Y
	FM56	06026-20-02	Y
	FM60	06026-23-02	Y
	FM23	06026-24-01	Y
	FM24	06026-24-02	Y
06066-XX-0X	FM30	06066-03-01	N
	FM47	06066-12-02	N
06095-XX-0X	FM32	06095-10-01	?
	FM63*	06095-10-02	?
	FM49	06095-21-01	?
	FM31*	06095-22-01	?
06244-XX-0X	None	None	?
06273-XX-0X	RPFM202	06273-01-02	?
	RPFM203*	06273-09-01	?

Table 6.6 — Astrium FM numbers and e2v serial numbers of FM CCDs likely to be affected by the SBC issue due to coming from affected batches (Y), likely to have fully functional SBCs due to coming from a likely unaffected batch (N) or not known because no CCDs from the batch have been tested for SBC efficiency (?), where * indicates flight spares.

Instrument	Number	Total	%	Affected
WFS	0	2	0	Y
	0	2	0	N
	2	2	100	?
BAM	0	2	0	Y
	0	2	0	N
	2	2	100	?
SM	3	14	21	Y
	0	14	0	N
	11	14	79	?
AF	15	62	24	Y
	2	62	3	N
	45	62	73	?
BP	0	7	0	Y
	0	7	0	N
	7	7	100	?
RP	0	7	0	Y
	0	7	0	N
	7	7	100	?
RVS	0	12	0	Y
	0	12	0	N
	12	12	100	?
All	18	106	17	Y
	2	106	2	N
	86	106	81	?

Table 6.7 — Summary of numbers of FM CCDs currently assigned to Gaia's FPA (see Fig. 6.16) likely to be affected by the SBC issue due to coming from affected batches (Y), likely to have fully functional SBCs due to coming from an unaffected batch (N) or not known because no CCDs from the batch have been tested for SBC efficiency (?).